Effective models of doped quantum ladders of non-Abelian anyons

Medha Soni, Matthias Troyer, and Didier Poilblanc

Phys. Rev. B **93**, 035124 — Published 21 January 2016

DOI: 10.1103/PhysRevB.93.035124

Effective models of doped quantum ladders of non-Abelian anyons

Medha Soni,[1] Matthias Troyer,[2] and Didier Poilblanc[1]

[1]*Laboratoire de Physique Théorique UMR-5152, CNRS and Université de Toulouse, F-31062 France*
[2]*Institut für Theoretische Physik, ETH-Hönggerberg, 8093 Zürich, Switzerland*

(Dated: November 23, 2015)

Quantum spin models have been studied extensively in one and higher dimensions. Furthermore, these systems have been doped with holes to study t–J models of $SU(2)$ spin-1/2. Their anyonic counterparts can be built from non-Abelian anyons, such as Fibonacci anyons described by $SU(2)_3$ theories, which are quantum deformations of the $SU(2)$ algebra. Inspired by the physics of $SU(2)$ spins, several works have explored ladders of Fibonacci anyons and also one-dimensional (1D) t–J models. Here we aim to explore the combined effects of extended dimensionality and doping by studying ladders composed of coupled chains of interacting itinerant Fibonacci anyons. We show analytically that in the limit of strong rung couplings these models can be mapped onto effective 1D models. These effective models can either be gapped models of hole pairs, or gapless models described by t–J (or modified t–J–V) chains of Fibonacci anyons, whose spectrum exhibits a fractionalization into charge and anyon degrees of freedom. The charge degrees of freedom are described by the hardcore boson spectra while the anyon sector is given by a chain of localized interacting anyons. By using exact diagonalizations for two-leg and three-leg ladders, we show that indeed the doped ladders show exactly the same behavior as that of t–J chains. In the strong ferromagnetic rung limit, we can obtain a new model that hosts two different kinds of Fibonacci particles - which we denote as the *heavy* τ's and *light* τ's. These two particle types carry the same (non-Abelian) topological charge but different (Abelian) electric charges. Once again, we map the two-dimensional ladder onto an effective chain carrying these heavy and light τ's. We perform a finite size scaling analysis to show the appearance of gapless modes for certain anyon densities whereas a topological gapped phase is suggested for another density regime.

PACS numbers: 75.10.Kt, 75.10.Jm, 75.40.Mg

I. INTRODUCTION

Quantum statistics is an important aspect of quantum mechanics and it lays down the rules for identifying different classes of particles. In three dimensions, the exchange of two particles in a quantum system can result in a phase change of either 0 or π for the wave function, leading to bosons and fermions. The scenario is very different in two-dimensions (2D) and it is well known that such quantum systems give rise to anyonic quasiparticle excitations.[1–3] These anyons are observed as excitations, localized disturbances of the ground state in systems with topological order. Rich behavior emerges especially for non-Abelian anyons, for which the exchange of two anyons is described by a unitary matrix.[4,5]

Models of interacting non-Abelian anyons draw motivation from quantum spin models, and in particular the Heisenberg model, which has been studied for a wide range of lattices including one-dimension (1D) chains and ladders of $SU(2)$ spins. Non-Abelian anyons can be described as so-called quantum deformations of the usual $SU(2)$ spins. Formally, they are described by $SU(2)_k$ Chern-Simons theories. These $SU(2)_k$ theories are obtained by 'deforming' the $SU(2)$ algebra so as to retain only the first $k+1$ representations. The most widely studied models are the $k=2$ and $k=3$ theories that describe 'Ising' and 'Fibonacci' anyons respectively.

Non-Abelian anyons are expected to be present in topologically ordered systems including certain fractional quantum Hall states,[6–9] p-wave superconductors,[10] spin models,[11–14] solid state heterostructures[15–20] and rotating Bose-Einstein condensates.[21] In particular, Fibonacci anyons occur as quasi holes in the $\mathbb{Z}_3$ Read-Rezayi state which might be able to describe the $\nu = 12/5$ fractional quantum Hall state.[22] While several experiments have shown evidence for emergent Majorana modes,[23–27] experimental evidence of Fibonacci anyons is yet to come.

In the absence of interactions, non-Abelian anyons have an exponentially degenerate ground state manifold. On this ground state manifold exchange (braiding) of non-Abelian anyons acts in a non-commutative way, by bringing about a non-trivial transformation in the degenerate manifold of the many-quasiparticle Hilbert space. This has generated interest since it can be used for topological fault-tolerant quantum computation.[28–33]

Interactions between non-Abelian anyons can be modeled by generalizations of the spin-1/2 Heisenberg model. These models have been studied for chains of Fibonacci anyons[34] including nearest neighbour couplings[35] and also longer range couplings[36] have been studied. Chains of higher spin quasiparticles have also been explored,[37–41] critical phases have been identified and the corresponding conformal field theory (CFT) has been obtained from numerical simulations.[42] The effect of disorder for chains of Fibonacci anyons has been investigated.[43,44]

As a step towards understanding the collective behavior of itinerant non-Abelian anyons, these chains can be doped with mobile holes, inspired by the electronic t–J model.[45–48] Electrons confined in 1D can exhibit the phenomenon of "spin-charge separation", where the spec-

trum can be interpreted in terms of two independent pieces, one arising from electric charge without spin, and the other from a spinon without any charge.[49] Analogously low-energy effective t–J models have been analyzed for the case of doped chains of Fibonacci (and Ising) anyons. These models exhibit a fractionalization of the spectrum into charge and anyonic degrees of freedom,[50,51] an extension of a phenomenon that exists in Luttinger liquids.[52–54]

As a step towards two dimensions, anyon models have been investigated on chains coupled to form so-called quantum *ladders* of non-Abelian anyons, which provide anyonic generalizations of the 2D quantum magnets.[55,56]

In this article, we would like to understand the physics of mobile non-Abelian anyons beyond one-dimension, which is a general fundamental and timely issue. Our aim is to construct the simplest possible model of 2D itinerant interacting anyons in close analogy to fermionic systems and inspired by the previous anyonic studies. As discussed later, this model takes the form of an anyonic 2D $t-J$ model very similar to its electronic 2D analog and to its 1D anyonic version mentioned above. Also a natural geometry to consider, interpolating between 1D and 2D, is the ladder geometry – e.g. a system of a finite number of coupled chains – used both for electronic spins and localized anyons. More precisely, we combine the anyonic models mentioned above, by studying *doped* quantum ladders of Fibonacci anyons consisting of two or three chains. In particular, we ask the question if spin-charge separation survives in the ladder model for non-Abelian anyons. Furthermore, in the study of this model, we have found a novel physical effective model that possibly hosts a topological gapped state.

The structure of the rest of the paper is as follows: Section II begins with a brief introduction of non-Abelian anyons and introduces our model. In section III A, we discuss the strong rung coupling limit drawing analogy with the spin ladder models, listing out all the possible quantum states and the phase diagram for the model under study. In section III B, we list all the phases that arise for weakly coupled rungs. The subsequent sections are dedicated to the discussion of all these phases. Section IV discusses the hard-core boson models and section V describes the golden chain phases. In section VI, we analyse the effective $t-J$ models for two and three-leg ladders, presenting the numerical results for the same. We extend the phenomenon of spin-charge separation to (doped) ladders of Fibonacci anyons. In section VII, we introduce a new model of heavy and light Fibonacci anyons that is obtained for certain density regimes when the rung couplings are FM. We conclude by summarising our results in section VIII.

II. THE MODEL

A. Introduction to non-Abelian anyons

In this paper we focus on Fibonacci anyons that are described by the $SU(2)_3$ theories. $SU(2)_k$ Chern-Simons theories[34,57] are so-called quantum deformations of the $SU(2)$ algebra. Their degrees of freedom are encoded by 'topological charges' j, which are generalized angular momenta. In contrast to $SU(2)$, in $SU(2)_k$ theories the total 'spin' j is limited to be $j = 0, \frac{1}{2}, \cdots, \frac{k}{2}$.

Akin to the tensor product of spins, non-Abelian anyons can be 'fused' according to fusion rules given by

$$j_1 \times j_2 = \sum_{j_3=|j_1-j_2|}^{min\{j_1+j_2,k-j_1-j_2\}} j_3. \tag{1}$$

For example, for the fusion of two anyons with $j_{1,2} = \frac{1}{2}$, these rules would mean $\frac{1}{2} \otimes \frac{1}{2} = 0 \oplus 1$ (for $k \geq 2$). Similarly, for the case of Fibonacci anyons ($k = 3$), when $j_{1,2} = 1$ the fusion rule reads as $1 \otimes 1 = 0 \oplus 1$. Note that this is different from what one would obtain under a tensor product of $SU(2)$ spin-1 particles. In the limit $k \to \infty$, however, we recover the $SU(2)$ algebra and the rule simply describes the tensor product of two ordinary $SU(2)$ spins.

In the rest of this manuscript, we focus only to the Fibonacci theory with $k = 3$, unless otherwise stated. There the allowed values for the topological charges are $j = 0, \frac{1}{2}, 1, \frac{3}{2}$. But if we look closely at the fusion rules, we can make the identification $0 \leftrightarrow \frac{3}{2}$ and $1 \leftrightarrow \frac{1}{2}$. Thus, the Fibonacci theory has two distinct types of *particles* which we denote as $\mathbf{1}$ for the trivial particle with $j = 0$ and τ for the Fibonacci anyon with $j = 1$ respectively. Using these, the fusion rules read

$$\begin{aligned} &\mathbf{1} \otimes \mathbf{1} = \mathbf{1} \\ &\tau \otimes \mathbf{1} = \mathbf{1} \otimes \tau = \tau \\ &\tau \otimes \tau = \mathbf{1} \oplus \tau. \end{aligned} \tag{2}$$

We represent a system of N anyons by means of a *fusion tree* as shown in Fig. 1(a), where the anyonic charges of the individual anyons are labelled by Y_i. The fusion outcome of successive fusion of the anyons are encoded by the 'bond' labels (links) in the fusion tree, labelled by x_i in Fig. 1(a). The constraints on the bond labels due to fusion rules which must be satisfied at each vertex significantly reduce the size of the internal Hilbert space. For N Fibonacci anyons (τ) the Hilbert space grows asymptotically as ϕ^N where $\phi = (\sqrt{5}+1)/2$ is the golden ratio. From now on we draw a flat version of the fusion tree, as shown in Fig. 1(b).

To perform an operation on nearest neighbor anyons, it is advantageous to change to a different basis in which the two-particle fusion outcome is explicit. This is done via the F-move shown schematically in Fig. 1(c). The F-move depends on the two site labels Y_i and Y_{i+1} and

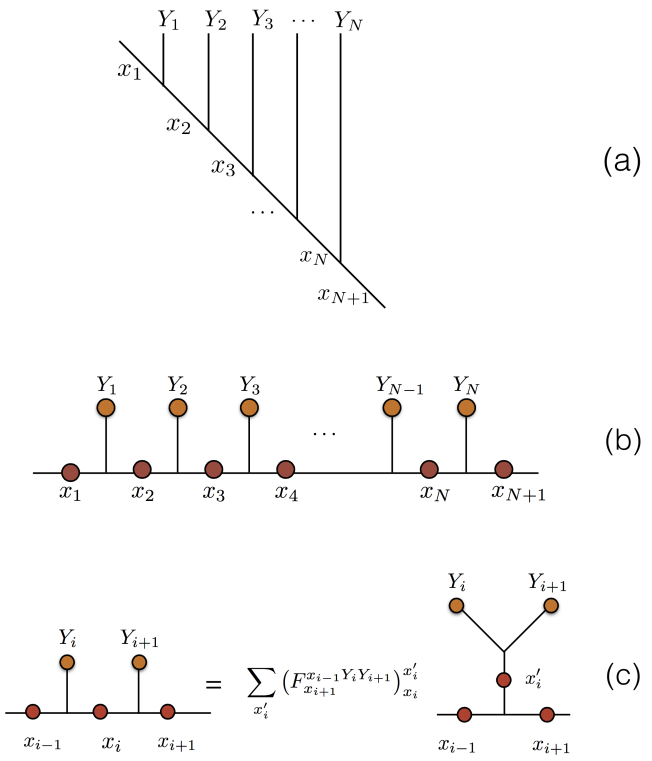

FIG. 1: (a) Illustration of the standard fusion tree with site labels Y_i (that can be either τ or $\mathbf{1}$) and bond labels x_i. (b) The flat version of the fusion tree. (c) A basis change to a different fusion tree using an F-move.

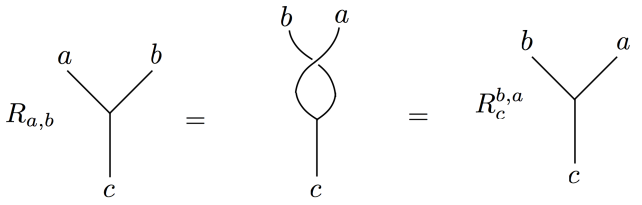

FIG. 2: Convention for the right handed braid to exchange two particles.

the bond labels x_{i-1} and x_{i+1}. If at least one of these four labels is $\mathbf{1}$, then there is only one choice of bond labels that satisfies the fusion algebra and the F-move is trivial. A non-trivial matrix is obtained only when all the four labels are τ anyons. Specialising to the case where $Y_i = Y_{i+1} = \tau$, the labels for the three bonds $|x_{i-1}, x_i, x_{i+1}\rangle$ allowed by the fusion rules are

$$\{|\mathbf{1},\tau,\mathbf{1}\rangle, |\mathbf{1},\tau,\tau\rangle, |\tau,\tau,\mathbf{1}\rangle, |\tau,\mathbf{1},\tau\rangle, |\tau,\tau,\tau\rangle\} \tag{3}$$

which transforms to a new basis $|x_{i-1}, x_i', x_{i+1}\rangle$ after the F-move:

$$\{|\mathbf{1},\mathbf{1},\mathbf{1}\rangle, |\mathbf{1},\tau,\tau\rangle, |\tau,\tau,\mathbf{1}\rangle, |\tau,\mathbf{1},\tau\rangle, |\tau,\tau,\tau\rangle\}.$$

Using these bases the F-matrix is represented as,

$$F = \begin{bmatrix} 1 & & & & \\ & 1 & & & \\ & & 1 & & \\ & & & \phi^{-1} & \phi^{-1/2} \\ & & & \phi^{-1/2} & -\phi^{-1} \end{bmatrix}, \tag{4}$$

where as mentioned above we have a non-trivial 2×2 submatrix only when also $x_{i-1} = x_{i+1} = \tau$.

Another operation that we need to perform on nearest neighbor anyons is that of exchanging (or braiding) them. In Fig. 2, we show our convention for a right-handed braid. The left-hand braiding is the inverse of the process shown here. Under a right-handed braid anyons a and b pick up a phase $R_c^{b,a}$ depending on the anyon types, a and b, that are undergoing an exchange and their fusion outcome c. Note that whenever a or b are $\mathbf{1}$, the phase is trivial. Non-trivial phases are only obtained are for $a = b = \tau$:

$$R_{\mathbf{1}}^{\tau\tau} = e^{+4\pi i/5}, R_{\tau}^{\tau\tau} = e^{-3\pi i/5}. \tag{5}$$

In order to implement a braid on the standard fusion tree, we first have to change basis using an F-move to make the fusion outcome of the two anyons explicit, and then braid. This process is shown schematically in Fig. 3. This is represented by a Braid matrix B acting on the bond labels $|x_{i-1}, x_i, x_{i+1}\rangle$. The only non-trivial Braid matrix is obtained when both the sites are occupied by τ anyons. In the basis of Eq. (3) we obtain:

$$B = FRF = \begin{bmatrix} e^{4i\pi/5} & 0 & 0 & 0 & 0 \\ 0 & e^{-3i\pi/5} & 0 & 0 & 0 \\ 0 & 0 & e^{-3i\pi/5} & 0 & 0 \\ 0 & 0 & 0 & \frac{1}{\phi^2}e^{4i\pi/5} + \frac{1}{\phi}e^{-3i\pi/5} & \frac{1}{\phi^{3/2}}(e^{4i\pi/5} - e^{-3i\pi/5}) \\ 0 & 0 & 0 & \frac{1}{\phi^{3/2}}(e^{4i\pi/5} - e^{-3i\pi/5}) & \frac{1}{\phi^2}e^{-3i\pi/5} + \frac{1}{\phi}e^{4i\pi/5} \end{bmatrix}. \tag{6}$$

Note that when the two site labels are a $\mathbf{1}$ and a τ, the F-moves and the exchange phases are all trivial. The

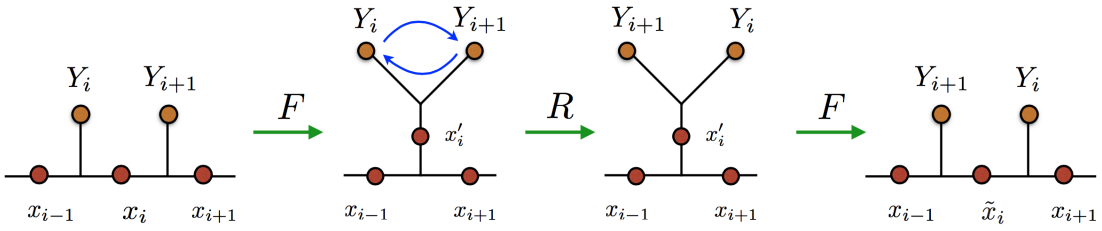

FIG. 3: Schematic representation of a braid on the fusion tree.

Braid matrix is effectively the hopping of the anyon to the adjacent site. When both the site labels are **1**, the Braid matrix is simply given by the identity matrix.

B. Golden chain model

In this section we review the so-called 'golden chains', consisting of 1D arrays of localized Fibonacci anyons with pairwise interactions between nearest neighbors.[35] In this model the Hamiltonian for the magnetic interactions between anyons is defined in analogy to the Heisenberg exchange interaction. We assign an energy $-J$ if the fusion outcome of two interacting anyons is trivial. For AFM couplings ($J > 0$), this favours the fusion outcome of two neighbouring anyons to be trivial, while for FM couplings ($J < 0$), the fusion of two anyons is preferred to be τ. This interaction between nearest neighbor anyons is depicted schematically in Fig. 4(a) and is implemented by projecting on the identity fusion channel

$$H_{\rm mag} = Jh_{\rm mag} = -J(FP^{\mathbf{1}}F^{-1}). \tag{7}$$

where F is the operator corresponding to the F-move (see Eq. (4)) and $P^{\mathbf{1}}$ is an operator that projects onto the **1** state. In the basis of Eq. (3), the matrix representation for the (dimensionless) magnetic interaction can be written explicitly as:

$$h_{\rm mag} = -\begin{bmatrix} 1 & & & & \\ & 0 & & & \\ & & 0 & & \\ & & & \phi^{-2} & \phi^{-3/2} \\ & & & \phi^{-3/2} & \phi^{-1} \end{bmatrix}. \tag{8}$$

Golden chains with AFM couplings are described by the $k = 3$ restricted solid on solid (RSOS) model which is a CFT with central charge $c = 7/10$. For ferromagnetic couplings the corresponding CFT is that of the critical 3-state Potts model with $c = 4/5$.[35,58]

C. Itinerant Fibonacci anyons in 1D

To model itinerant anyons we introduce holes, *i.e.* sites with a trivial anyon **1** on some of the sites. The holes and τ anyons are labelled by different $U(1)$ (electric) charges and anyonic (non-Abelian) charges. The τ anyons (referred to simply as 'anyons' or 'τ particles' hereafter) can move on the chain which results in an additional kinetic energy contribution. This kinetic process is schematically shown in Fig. 4(b). It involves the hopping of a particle, along with its electric and anyonic charge to a neighbouring site.

Our specific model of itinerant anyons is a generalization of the electronic t–J model.[45] Assuming a large on-site charging energy, we eliminate the possibility of doubly occupied sites and allow anyons to only hop to empty sites. As in the case of electrons, the low-energy effective t–J model allows hopping of the anyons to nearest neighbor vacant sites and an exchange interaction between nearest neighbor anyons analogous to the Heisenberg interactions explained above in Sec. II B. The kinetic term can then be written as $H_{\rm kin} = -th_{\rm kin}$, where $h_{\rm kin}$ is the (dimensionless) operator corresponding to the nearest neighbor hopping process shown in Fig. 4(b). A t–J chain of itinerant anyons was studied for Ising and Fibonacci anyons,[50,51] revealing a separation of excitations into charge and anyonic excitations, similar to spin-charge separation in its electronic counterpart.

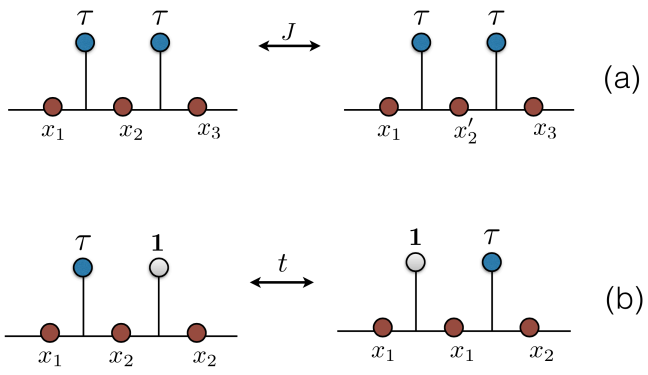

FIG. 4: (a) Nearest neighbor magnetic interaction of amplitude J. (b) The kinetic hopping (of amplitude t) of an anyon to its nearest neighbor vacant site. The blue circles represent τ anyons while the white circles denote vacant sites or holes.

D. Ladders of Fibonacci anyons

1. Undoped ladders

Ladders of Fibonacci anyons are formed by coupling chains of localized anyons.[55] Anyons interact with their nearest neighbors along the leg and rung directions via $J_{\rm leg}$ and $J_{\rm rung}$. These interactions are shown schematically in Fig. 5(a). As fusion path we choose the *zig-zag path* shown in Fig. 5(b), since it minimizes the effective range of interactions on the fusion path. We choose periodic boundary conditions along the leg direction and open boundary conditions along the rungs.

With this choice of fusion path, nearest neighbor interactions on the rungs are also nearest neighbor along the fusion path, while those between anyons on the same leg are longer range along the fusion path. Nearest neighbor rung interactions can be implemented in exactly the same way as for nearest neighbor on a chain (see Sec. II B). In order to evaluate the interactions between τ particles on the same leg, we have to implement a change of basis, this time by braiding them in a clockwise manner until they are neighbours along the fusion path. This braiding is performed by the unitary braid matrix B (see Eq. (6)). Once the τ particles are nearest neighbours along the path they can interact with the same term as discussed above in Sec. II B. After carrying out the interaction, the anyons have to be braided back to their original positions.

More specifically, for a two-leg ladder, adjacent anyons along the leg direction are next nearest neighbours along the fusion path (see Fig. 5(b)). Thus, one needs to implement one braid operation. The Hamiltonian for the magnetic interactions between nearest neighbor rungs r and $r+1$ on the upper leg is given by

$$(H^1_{\rm mag})_r = J_{\rm leg} B^\dagger_{2r-1} (h_{\rm mag})_{2r} B_{2r-1}, \qquad (9)$$

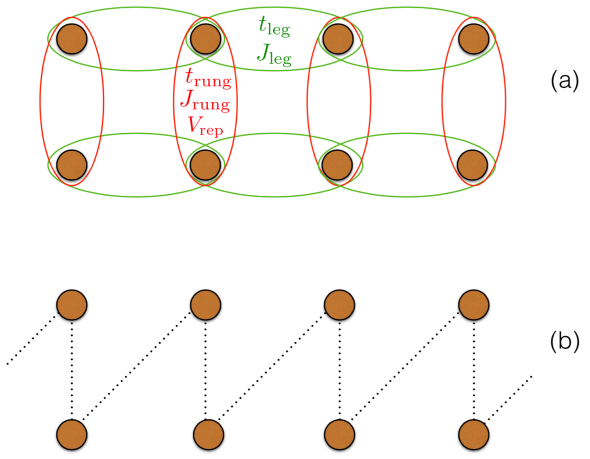

FIG. 5: Two-leg ladder: (a) Interactions along the leg and rung directions. (b) The zig-zag fusion path. The couplings have been indicated.

and on the lower leg as

$$(H^2_{\rm mag})_r = J_{\rm leg} B^\dagger_{2r+1} (h_{\rm mag})_{2r} B_{2r+1}, \qquad (10)$$

where $h_{\rm mag}$ has been defined in Eq. (8) and r labels the rungs (so that $i = 2r$ labels the diagonal bonds along the path). In Fig. 6(a), we summarize the magnetic interactions between nearest neighbor along the leg direction for a two-leg ladder.

For a three-leg ladder, the leg interactions are longer ranged interactions, since adjacent anyons on a leg are third neighbours along the fusion path. Thus, nearest neighbor leg interactions on a three-leg ladder ladder require two braids before particles are nearest neighbors on the fusion path.[55] One gets for interaction between rungs r and $r+1$ on the upper leg,

$$(H^1_{\rm mag})_r = J_{\rm leg} B^\dagger_{3r-2} B^\dagger_{3r-1} (h_{\rm mag})_{3r} B_{3r-1} B_{3r-2}, \qquad (11)$$

on the middle leg,

$$(H^2_{\rm mag})_r = J_{\rm leg} B^\dagger_{3r+1} B^\dagger_{3r-1} (h_{\rm mag})_{3r} B_{3r-1} B_{3r+1}, \qquad (12)$$

and on the lower leg,

$$(H^3_{\rm mag})_r = J_{\rm leg} B^\dagger_{3r+2} B^\dagger_{3r+1} (h_{\rm mag})_{3r} B_{3r+1} B_{3r+2}, \qquad (13)$$

where $i = 3r$ labels the diagonal bonds along the path.

The full magnetic Hamiltonian on the legs is obtained by adding all contributions, $H^{\rm leg}_{\rm mag} = \sum_1^W H^l_{\rm mag}$, where W is the number of legs. As an implementation detail we want to mention that the action of the operator $H^l_{\rm mag}$ can generate up to 2^{2W-1} states for each bond interaction. The operator mixes spin labels, thus generates multiple images for each two-body interaction. This exponential increase in the number of resulting states leads to denser Hamiltonian matrices as one increases the width W of the ladder and restricts us from exploring larger system sizes.

For ladders of Fibonacci anyons it was shown that similar odd-even effects as seen for $SU(2)$ spins continue to exist in the limit of strong AFM rungs.[55] AFM coupled ladders of Fibonacci anyons with even number of legs are gapped while those with odd number of legs are critical and are described by the same CFT as the golden chain. On the other hand, Fibonacci ladders with FM rung couplings are quite different from their $SU(2)$ counterparts.[55] Fibonacci ladders with a width that is a multiple of three are gapped since the rungs form singlets ($j = 0$). Other widths are gapless since the isolated rungs effectively form τ's, thereby yielding a gapless chain as the effective low-energy model. This is different from $SU(2)$ spins, for which an even number form a singlet ground state, and where thus all even width ladders are gapped.

2. Doped ladders

In this paper we focus on itinerant ladders of Fibonacci anyons. As schematically represented in Fig. 5(a) we denote the interaction strengths along the leg direction by

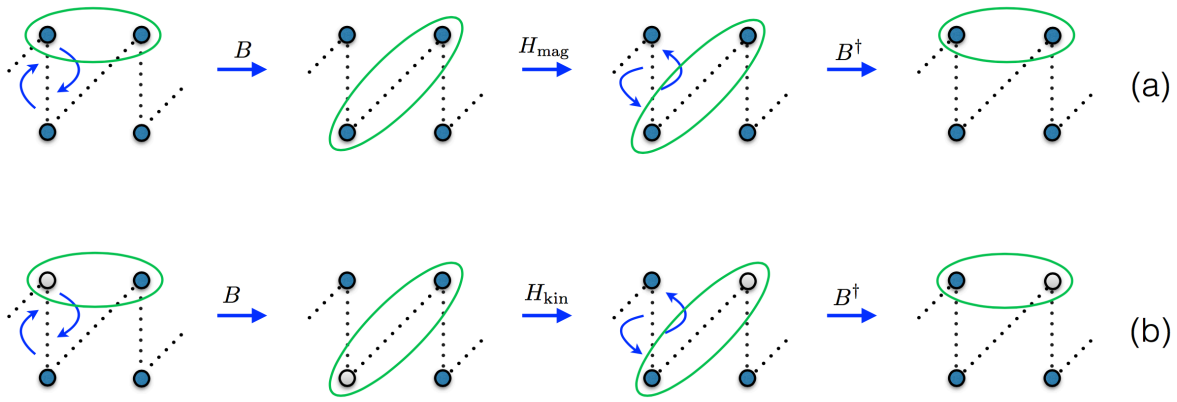

FIG. 6: Evaluation of Hamiltonian terms on a two-leg ladder along the leg direction that involve the braid operation. The blue circles represent τ particles white the white circles are for vacant sites. The green ellipses denote the particles that are interacting along the leg direction. (a) the magnetic term (b) the kinetic term.

$J_{\rm leg}$ and $t_{\rm leg}$ for the magnetic and kinetic terms respectively. Along the perpendicular direction, the couplings $J_{\rm rung}$ and $t_{\rm rung}$ denote respectively the magnetic and kinetic terms.

The magnetic interactions for the ladder have already been described in the section II D 1 and we thus only need to discuss the kinetic terms. Once again, the two sites on a rung are adjacent on the fusion path and the hopping is thus implemented as for the 1D t–J chain (see section II C). For a τ particle and hole lying on adjacent sites on the same leg of the ladder, we need to, once again, braid the sites to bring them to adjacent positions on the fusion tree. For a two-leg ladder, the kinetic term between rungs r and $r+1$ on the upper leg is given by

$$(H^1_{\rm kin})_r = t_{\rm leg} B^\dagger_{2r-1} (h_{\rm kin})_{2r} B_{2r-1}, \tag{14}$$

and on the lower leg as

$$(H^2_{\rm kin})_r = t_{\rm leg} B^\dagger_{2r+1} (h_{\rm kin})_{2r} B_{2r+1}, \tag{15}$$

where $h_{\rm kin}$ has been defined above and r labels the rungs. In Fig. 6(b), we summarize the kinetic process between nearest neighbor sites along the leg direction for a two-leg ladder.

For a three-leg ladder, a τ particle and hole lying on adjacent sites on a leg are third neighbours along the fusion path. Thus, nearest neighbor leg interaction on a three-leg ladder requires two braids before the τ particle and the hole are nearest neighbors on the fusion path. One gets for kinetic terms between rungs r and $r+1$ on the upper leg,

$$(H^1_{\rm kin})_r = t_{\rm leg} B^\dagger_{3r-2} B^\dagger_{3r-1} (h_{\rm kin})_{3r} B_{3r-1} B_{3r-2}, \tag{16}$$

on the middle leg,

$$(H^2_{\rm kin})_r = t_{\rm leg} B^\dagger_{3r+1} B^\dagger_{3r-1} (h_{\rm kin})_{3r} B_{3r-1} B_{3r+1}, \tag{17}$$

and on the lower leg,

$$(H^3_{\rm kin})_r = t_{\rm leg} B^\dagger_{3r+2} B^\dagger_{3r+1} (h_{\rm kin})_{3r} B_{3r+1} B_{3r+2}, \tag{18}$$

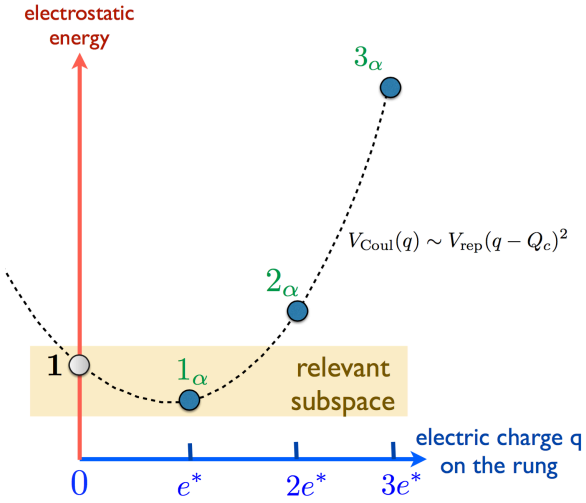

FIG. 7: Schematic energy spectra in the presence of a parabolic Coulombic charging energy. One can tune the chemical potential and the repulsion between the particles in order to gap out the higher energy sectors. This allows restricting the calculations to a low energy subspace.

where $i = 3r$ labels the diagonal bonds along the path.

Note that, in the above equations, some of the braids may be trivial, in contrast to the case of the magnetic interactions. The full kinetic Hamiltonian on the legs is obtained by adding all contributions, $H^{\rm leg}_{\rm kin} = \sum_1^W H^l_{\rm kin}$. Here, the action of the operator $H^l_{\rm kin}$ can generate up to 2^{2W-2} states for each bond interaction.

We also consider models with an additional rung charging term

$$V_{\rm Coul}(q) \sim V_{\rm rep}(q - Q_c)^2, \tag{19}$$

where q is the number of anyons on a rung and Q_c is determined by the implicit chemical potential. Fig. 7 shows the energy profile for a given rung composition on the

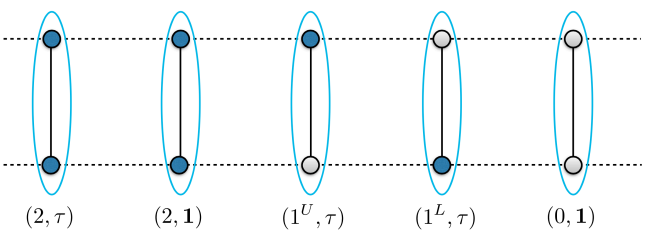

FIG. 8: All possible fusion outcomes for a rung of a two-leg ladder. The blue circles represent τ's while white circles represent vacant sites. The $U(1)$ and topological charges for the different configurations are denoted in the parenthesis. The superscript $U(L)$ refers to the τ lying on the upper (lower) leg.

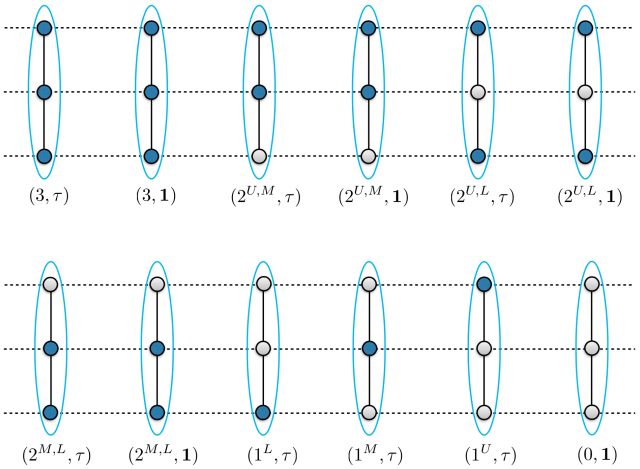

FIG. 9: The various fusion outcomes possible for a doped three-leg ladder. The blue circles represent τ's while white circles represent vacant sites. The first labels in the parenthesis signify the $U(1)$ charge, corresponding to the number of τ's present on each rung and the second refers to their fusion outcome. The superscripts U, M, L refer to the positions of the τ on the different legs (upper, middle, lower) of the ladder.

ladder. For the three-leg ladder under consideration, this term acts pairwise between all the three possible pairs of particles that can exist on the three-site rung. Assuming a charging energy which is much larger compared to the exchange energy, we can consider the limit $V_{\rm rep} \to \infty$. In this limit we can restrict our calculations to just two values of the occupation on the rung, n and $n+1$, with n ranging from 0 to $W-1$. This reduces the Hilbert space and thus allows us to perform simulations of larger ladders.

E. Simulation algorithm

Our numerical simulations have been performed by exact diagonalization using the Lanczos algorithm. We exploit periodic boundary conditions along the leg direction to implement translation symmetry. This allows us to block-diagonalize the Hamiltonian into L blocks labeled by the total momentum $K = 2\pi\frac{m}{L}$ (m being an integer), which reduces the size of the Hilbert space, which is the major limiting factor in the simulations, by a factor L.

III. PHASE DIAGRAMS

A. Isolated rung limit

Analogous to standard electronic t–J ladders the physics of anyonic t–J ladders can be understood starting from the strong rung coupling limit.[59,60] We thus begin by identifying the low-lying states of isolated rungs.

In Fig. 8, we show the five rung configurations on isolated rungs for a two-leg ladder, and the total $U(1)$ and anyonic charges that are possible for these rung configurations. When there are two holes on a rung, both of these charges are trivially zero. When the rung is occupied by two τ particles, the net $U(1)$ charge is 2, however the topological charge may be either $\mathbf{1}$ or τ, giving rise to two different quantum states $|2,\tau\rangle$ (named "heavy τ") and $|2,\mathbf{1}\rangle$ (named "heavy hole" – an empty rung being a "light hole"). In the case when there is a single τ on the rung, it can be either on the upper or on the lower leg with charges denoted as $(1^U,\tau)$ and $(1^L,\tau)$ respectively. The corresponding quantum states are respectively $|1^U,\tau\rangle$ and $|1^L,\tau\rangle$. The bonding and anti-bonding states $|1^\pm,\tau\rangle$ (named "light τ") are formed by linear superpositions of the configurations with charges $(1^U,\tau)$ and $(1^L,\tau)$ given by

$$|1^\pm,\tau\rangle = \frac{1}{\sqrt{2}}\big(|1^U,\tau\rangle \pm |1^L,\tau\rangle\big)\,. \tag{20}$$

For a three-leg ladder, many more states are possible, as shown in Fig. 9. When there is a single τ on the rung ($N_{\rm rung} = 1$), the "light τ" quantum states formed by linear superpositions of the three different positions of the τ particle are given by

$$|1^\pm,\tau\rangle = \frac{1}{2}\big(|1^U,\tau\rangle + |1^L,\tau\rangle \pm \sqrt{2}|1^M,\tau\rangle\big)\,, \tag{21}$$

$$|1^0,\tau\rangle = \frac{1}{\sqrt{2}}\big(|1^U,\tau\rangle - |1^L,\tau\rangle\big)\,. \tag{22}$$

Depending on the sign of the hopping, one of the states $|1^\pm,\tau\rangle$ acquires the lowest energy. Likewise, when there are two τ anyons on a rung ($N_{\rm rung} = 2$) we can form quantum states as linear superpositions of the states with the same $U(1)$ and topological charges. For $J_{\rm rung} > 0$, one of the "heavy hole" states

$$|2^\pm,\mathbf{1}\rangle = \frac{1}{\sqrt{2+\alpha^2}}\big(|2^{U,M},\mathbf{1}\rangle + |2^{M,L},\mathbf{1}\rangle \pm \alpha|2^{U,L},\mathbf{1}\rangle\big) \tag{23}$$

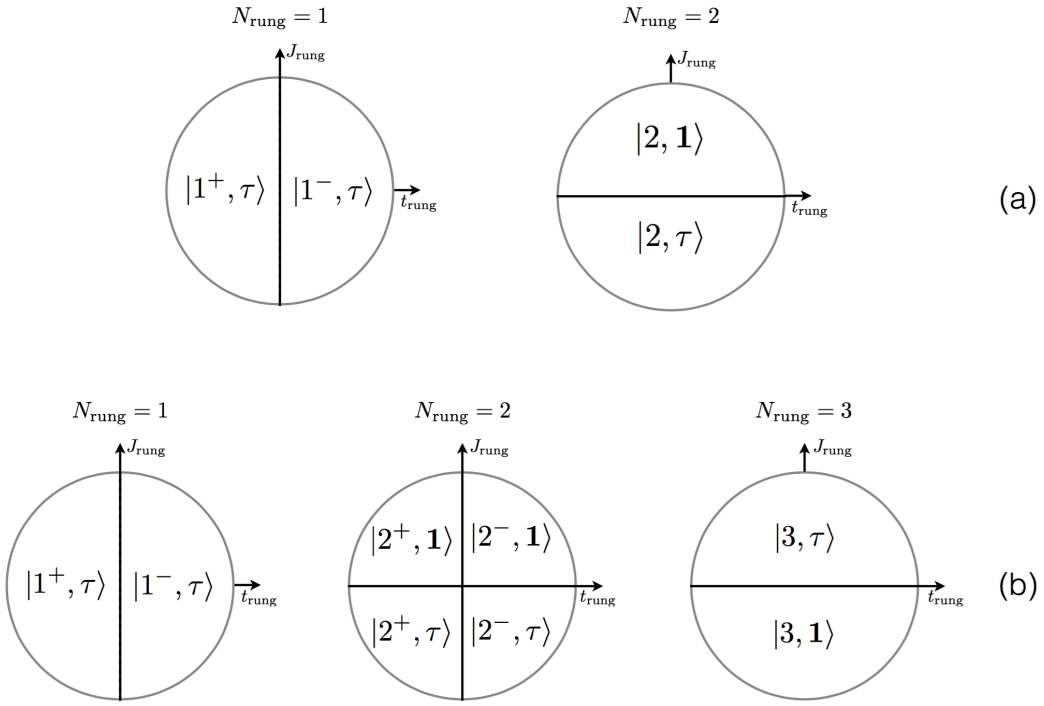

FIG. 10: Ground state phase diagram for (a) two-leg ladder and (b) three-leg ladder in the isolated rung limit (with or without charging energy). The lowest energy sectors for isolated rungs with different anyon numbers (labelled by $N_{\rm rung}$) on a ladders of itinerant Fibonacci anyons are indicated. The notations are the same as in Figs. 8 and 9.

is the ground state, with

$$\alpha = \frac{\sqrt{J_{\rm rung}^2 + 8t_{\rm rung}^2} - J_{\rm rung}}{2t_{\rm rung}}. \tag{24}$$

If for simplicity, we consider $J_{\rm rung} = t_{\rm rung}$, then $\alpha = 1$. For $J_{\rm rung} < 0$ either of the "heavy τ" states

$$|2^{\pm},\tau\rangle = \frac{1}{2}\big(|2^{U,M},\tau\rangle + |2^{M,L},\tau\rangle \pm \sqrt{2}|2^{U,L},\tau\rangle\big) \tag{25}$$

has lowest energy depending on the sign of the hopping $t_{\rm rung}$. When the rung is occupied by three τ particles, the total $U(1)$ charge on the rung is 3, and the possible quantum states are $|3,\tau\rangle$ (named "super-heavy" τ) and $|3,\mathbf{1}\rangle$ (named "super-heavy hole") depending on the net fusion outcome.

In the limit of independent rungs and by parametrising the rung couplings as $t_{\rm rung} = \cos\theta$ and $J_{\rm rung} = \sin\theta$, we have mapped out the parameter space on a unit circle. In Fig. 10 we show the ground state phase diagram for an isolated rung on a two-leg or a three-leg ladder for different number $N_{\rm rung}$ of τ anyons on the rung. Note that these phase diagrams do not depend on the charging energy which only gives a constant energy shift $V_{\rm rep}(N_{\rm rung}e^* - Q_c)^2$ (depending on the $N_{\rm rung}$ sector).

B. Phase diagrams of weakly coupled rungs

Our goal is now to understand the phase diagram of anyonic ladders by starting from the isolated rung coupling limits. We do this by turning on small couplings $t_{\rm leg}$ and $J_{\rm leg}$ between the strongly coupled rungs such that $|t_{\rm leg}|, |J_{\rm leg}| << |t_{\rm rung}|, |J_{\rm rung}|$, in order to ensure that there is no transition to excited state of the isolated rungs. Figures 11 and 12 summarize the phase diagrams for two and three-leg ladders.

Depending on the low-energy states on each rung we find six different types of phases:

- Totally gapped phases (T) appear when there are exactly two (for $J_{\rm rung} > 0$) or three (for $J_{\rm rung} < 0$) anyons per rung that fuse into the trivial channel. These phases will not be discussed further.
- Effective golden chains ($G^{\pm}$) when there are exactly n τ anyons on every rung that fuse into a total τ. An optional $\pm$ superscript indicates whether the particles are in a bonding (+) or antibonding(−) state on a rung. These phases will be discussed in Sec. V.
- Paired phases (P) where two anyons on a rung fuse in the trivial channel, forming hard-core bosons. These phases will be discussed in Sec. IV
- Effective t–J chains ($C^{\pm}_{nm}$) consisting of an effective hole that arises from n anyons on a rung fusing in

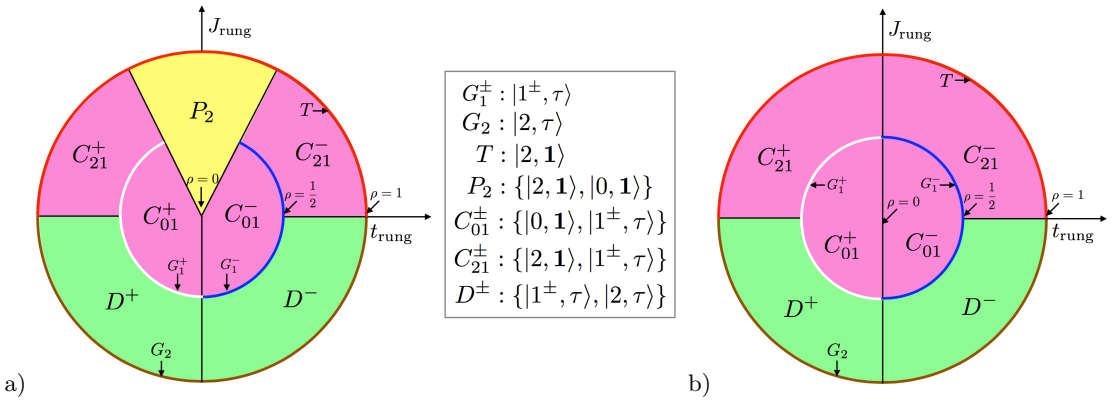

FIG. 11: Phase diagrams of the two-leg ladder in the strong rung coupling limit. a) is without a rung charging term and b) with a large rung charging term $V_{\rm rep}$. Here the radius denotes the density of anyons. Depending on filling and coupling several phases can be distinguished: a totally gaped phase (T), effective golden chain models (G), effective t–J chains (C), paired phases (P), and a phase with two different types of τ anyons (D). The legend indicates which rung states are relevant in the various phases. See the text for details.

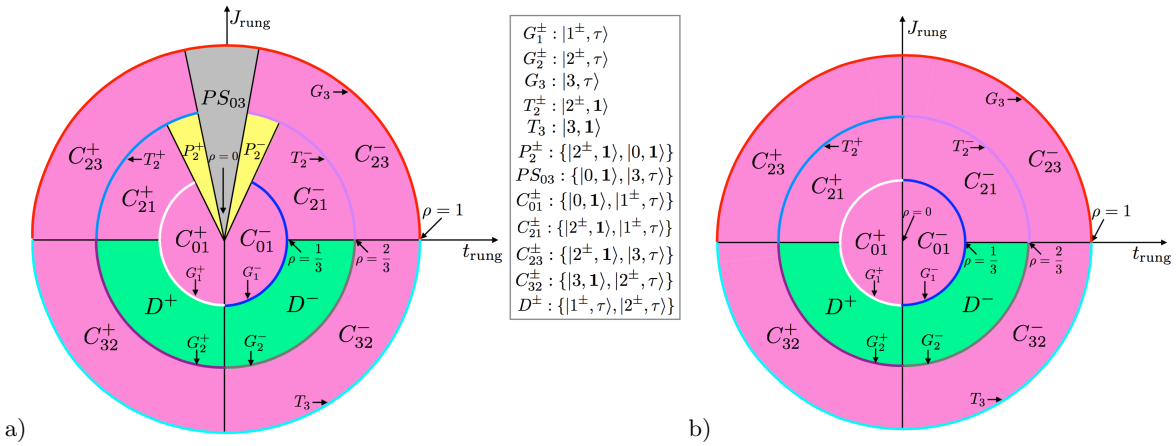

FIG. 12: Phase diagrams of the three-leg ladder in the strong rung coupling limit. a) is without a rung charging term and b) with a large rung charging term $V_{\rm rep}$. Here the radius denotes the density of anyons. Depending on filling and coupling several phases can be distinguished: a totally gaped phase (T), effective golden chain models (G), effective t–J chains (C), paired phases (P), phase separated phases (PS) and a phase with two different types of τ anyons (D). The legend indicates which rung states are relevant in the various phases. See the text for details.

the trivial channel and an effective τ anyon arising from m anyons fusing in the τ channel. The $\pm$ superscript indicates whether the particles on a rung are in a bonding or antibonding state. These phases will be discussed in Sec. VI

- Effective models consisting of two flavors of τ anyons ($D_{mn}^\pm$) that are formed by fusing m and n anyons on a rung respectively. Again the $\pm$ superscript indicates whether the particles on a rung are in a bonding or antibonding state.

- A phase separated region PS_{03} originated from an effective t–J chain with dominant attraction between the effective super-heavy τ anyons.

The effect of a large rung charging energy $V_{\rm rep}$ is to suppress pairing and phase separation in two-leg and three-leg ladders. The other phases are unchanged when adding this term. We will thus use $V_{\rm rep}=\infty$ to reduce the Hilbert space dimension when numerically investigating the latter phases.

IV. PAIRING AND EFFECTIVE HARD-CORE BOSON MODELS

We start our detailed discussion with paired phases that arise when two τ anyons on a rung fuse into an effective trivial particle and are then described by mobile hard core bosons. In the case of the two-leg ladder this phase appears when $J_{\rm rung} > 2|t_{\rm rung}|$. Identifying $|0,\mathbf{1}\rangle$ with an empty site and $|2,\mathbf{1}\rangle$ with a hard-core boson we

end up with an effective hard-core boson (HCB) model,

$$H_{\rm HCB} = t\sum_i (b_i^\dagger b_{i+1} + h.c.) + V\sum_i n_i(1-n_{i+1}), \quad (26)$$

where $b_i^\dagger$ creates a boson at site i and $n_i = b_i^\dagger b_i$ is the boson density. The effective hopping matrix element of this hard-core boson model is obtained from second-order perturbation theory in $t_{\rm leg}$ to be

$$t = -\frac{2t_{\rm leg}^2}{J_{\rm rung} - 2|t_{\rm rung}|}. \quad (27)$$

An effective nearest neighbor attraction between different types of holes comes also in second-order and is given by

$$V = -\frac{2t_{\rm leg}^2}{J_{\rm rung} - 2|t_{\rm rung}|}. \quad (28)$$

This is similar to fermionic t–J ladders mapping to a Luther-Emery liquid of Cooper pairs.

In the three leg ladder, similar paired phases described by the same hard-core boson model are found when $\rho < 2/3$ and the rung couplings satisfy

$$3\phi|t_{\rm rung}| > J_{\rm rung} > \frac{3}{\sqrt{2}}|t_{\rm rung}|\,. \quad (29)$$

The effective hopping matrix element of this hard-core boson model is

$$t = -\frac{2t_{\rm leg}^2}{E_D}, \quad (30)$$

where $E_D = -2\sqrt{2}|t_{\rm rung}| + \frac{J_{\rm rung}}{2} + \frac{\sqrt{J_{\rm rung}^2+8t_{\rm rung}^2}}{2}$ and a proof is provided in Eq. (A74). An additional effective attraction between different types of holes is given by

$$V = -\frac{2t_{\rm leg}^2}{E_D}, \quad (31)$$

as shown in Eq. (A73).

V. EFFECTIVE GOLDEN CHAINS

If all rungs are at the same integer filling n, the effective model is either in a trivial gapped phase if the n anyons fuse into the trivial channel, or an effective golden chain model if they form a total τ. We label the latter phases as G_n or $G_n^\pm$, where the optional $\pm$ index indicates whether the anyons are in a bonding state (+) or antibonding state (−) on the rung.

The phase $G_1^\pm$ appears in the two-leg ladder at unit filling (outside of the paired phase). With two τ particles per rung and $J_{\rm rung} < 0$ we obtain the phase G_2.

Analogously, the three leg ladder has effective golden chain phases for specific densities $\rho = 1/3, 2/3, 1$ on the ladder. In the case when all the rungs have exactly one τ particle, the phase $G_1^\pm$ is obtained. When there are two τ anyons per rung and $J_{\rm rung} < 0$, the phase $G_2^\pm$ appears. Finally, for three τ particles per rung and $J_{\rm rung} > 0$, we obtain the G_3 phase.

All coupling constants J of the effective Golden chains are listed in Table I.

TABLE I: Effective couplings for the various golden chain phases as a function of the ladder width W and density ρ.

W	ρ	Phase	$J/J_{\rm leg}$	Derivation Eq.
2	$\frac{1}{2}$	$G_1^\pm$	$\frac{1}{2}$	(A4)
2	1	G_2	$\frac{2}{\phi^2}$	(A12)
3	$\frac{1}{3}$	$G_1^\pm$	$\frac{3}{8}$	(A21)
3	$\frac{2}{3}$	$G_2^\pm$	$\frac{11}{8\phi^2}$	(A25)
3	1	G_3	1	(A30)

VI. EFFECTIVE t–J MODELS

A. Two-leg ladder

1. *Effective t–J models*

Doping the $\rho = 1/2$ $G_1^\pm$ golden chain with (light) holes one obtains an effective anyonic t–J chain ($C_{01}^\pm$). The magnetic coupling J is the same as for the $G_1^\pm$ golden chain.

Increasing the U(1) charge density ($\rho > 1/2$), by effectively doping the $G_1^\pm$ golden chain with heavy holes, one obtains a similar $C_{21}^\pm$ $t-J$ chain for AFM rung couplings $J_{\rm rung} > 0$ with a sign change of the hopping term.

Coupling constants are summarized in Table II.

2. *Effective model for charge degrees of freedom*

From the mapping of a doped ladder to an effective 1D t–J chain we expect its spectrum to fractionalize into charge and anyon (called also "spin") degrees of freedom. To investigate spin-charge separation in the ladder, we first examine the pure $U(1)$ charge spectrum when $J_{\rm leg} = 0$.

In the $J = 0$ limit of an anyoninc t–J chain the itinerant anyons behave like HCBs which can be mapped onto

TABLE II: Effective couplings for the various t–J phases of the two-leg ladder as a function of the density ρ.

Filling	Phase	$J/J_{\rm leg}$	$t/t_{\rm leg}$	Derivation Eq.
$\rho < \frac{1}{2}$	$C_{01}^\pm$	$\frac{1}{2}$	$\frac{1}{2}$	(A37)
$\rho > \frac{1}{2}$	$C_{21}^\pm$	$\frac{1}{2}$	$-\frac{1}{2}$	(A42)

a system of spinless fermions. Adding an external flux in the ring, the HCB spectrum is therefore given by charge excitation parabolas,

$$E_{\rm HCB}(p,\phi_{\rm ext}) = -2t\sum_{j(p)}\cos\left[\frac{2\pi}{L}\left(j+\frac{1}{2}\right)+\frac{\phi_{\rm ext}}{L}\right], \quad (32)$$

where $\{j(p)\}$ is a set of integers (labelled by the branch index p) which determine the continuous momenta, given by $K = \frac{2\pi}{L}\sum_{j(p)}(j+\frac{1}{2}) + \tilde{\rho}\phi_{\rm ext}$, $\tilde{\rho}$ being the density of particles in the system. In the $J=0$ limit we must be careful since the fusion tree labels make the anyons distinguishable. Thus, in the absence of magnetic interactions the energy levels show a high degree of degeneracy that arises due to the built in non-Abelian nature of the Fibonacci anyons. Moving an anyon across the boundary cyclically translates the fusion tree labels. All N particles must be translated over the boundary to be able to have the original labeling. This brings about a phase shift of $\phi_n = 2\pi n/N$, n being an integer. The charge spectrum of the anyonic chain can then be described as a union of all HCB spectra for all discrete values of ϕ_n, with no external flux:

$$E^{p,n}_{\rm charge} = E_{\rm HCB}(p,\phi_n). \quad (33)$$

The states are labelled by their total momentum $K_{p,n} = K_p + 2\pi\frac{n}{N}$.

Our numerical results show that, as expected, the charge spectrum of the ladder corresponds exactly to that of the effective chain. As an example, Fig. 13 shows the $J_{\rm leg}=0$ spectrum of a 2×8 ladder with $\rho = 3/4$, which

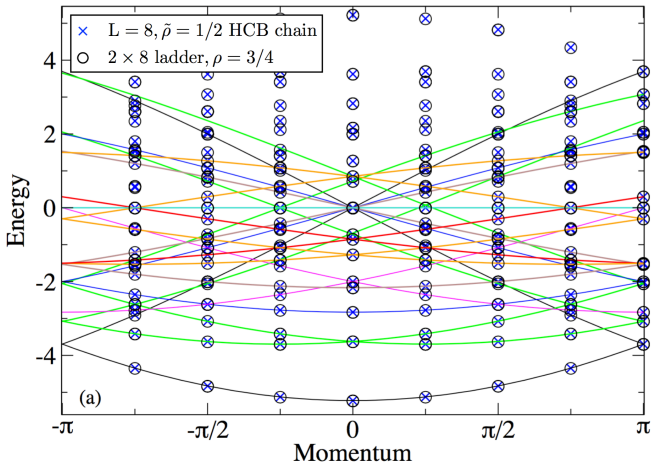

FIG. 13: Charge spectrum at $J_{\rm rung} = t_{\rm rung} = 1000, t_{\rm leg} = 1, J_{\rm leg} = 0, V_{\rm rep} = \infty$. The solid lines denote the HCB spectrum (with an external flux) given by Eq. (32), different colors corresponding to the different charge branches (labelled by p in Eq. (32). The black circles denote the spectrum of a 2×8 ladder with $\rho = 3/4$. The blue crosses correspond to the effective chain spectrum for $L=8$, $\tilde{\rho}=1/2$ (see Eq. (33)).

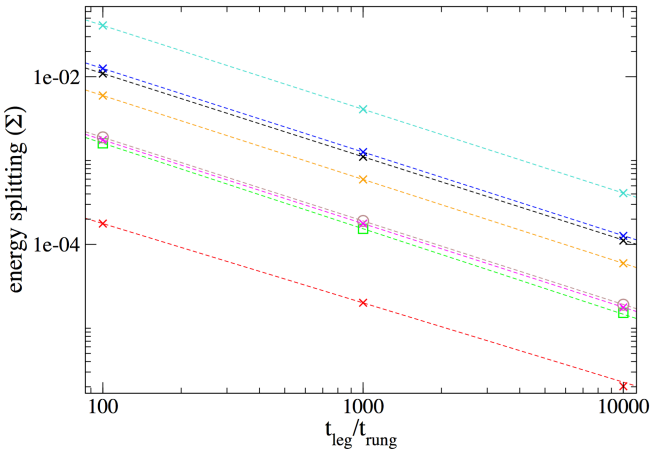

FIG. 14: Energy splittings of each of the eight $E \le 0$ energy levels at $K=0$ of the 2×8 ladder with $\rho = 3/4$ (symbol/line colors here match the colors of the parabolic branches of Fig. 13) as a function of $t_{\rm leg}/t_{\rm rung}$. The values of the leg couplings are $t_{\rm leg}=1, J_{\rm leg}=0, V_{\rm rep}=\infty$ and $t_{\rm rung}(=J_{\rm rung})$ takes different values from 100 to 10000. The fits correspond to the expected $t^{-1}_{\rm rung}$ behavior.

is in perfect agreement with the spectrum of an effective $J=0$ chain with $L=8$ and $\tilde{\rho}=1/2$ and with the HCB spectrum given by the cosine branches according to Eqs. (32) and (33). Note that there is a global shift in energy between the ladder and the chain spectra given by

$$E_{\rm shift} = -t_{\rm rung}N_s - J_{\rm rung}N_d, \quad (34)$$

where N_s (N_d) are the number of rungs carrying a single (two) τ (s).

Lastly, we would like to mention that the mapping is exact only in the limit when the rung couplings tend to infinity. For large, yet finite, rung couplings the energy levels of the ladder model in each parabola are split into an exponential number of energy levels over a finite energy range Σ. This is due to second order processes to higher energy states that give rise to a broadening of order $\Sigma \sim t^2_{\rm leg}/t_{\rm rung}$ and $t^2_{\rm leg}/J_{\rm rung}$ of the energy levels, as shown in Fig. 14.

3. *Numerical comparison between microscopic model and 1D t-J model*

We next turn on a small $J_{\rm leg}$ and adiabatically follow the splitting of the charge parabolas. Fig. 15(a) zooms into the low energy spectrum to show how the highly degenerate energy levels are split by a small $J_{\rm leg}=0.1$. Fig. 15(b) shows results for a larger coupling $J_{\rm leg}=1$. We see that magnetic interactions lift the degeneracy of the states with an energy spread proportional to $LJ_{\rm leg}$. This is consistent with the behavior of the effective t–J chain exhibiting "spin-charge separation": in Refs. 50,51 we

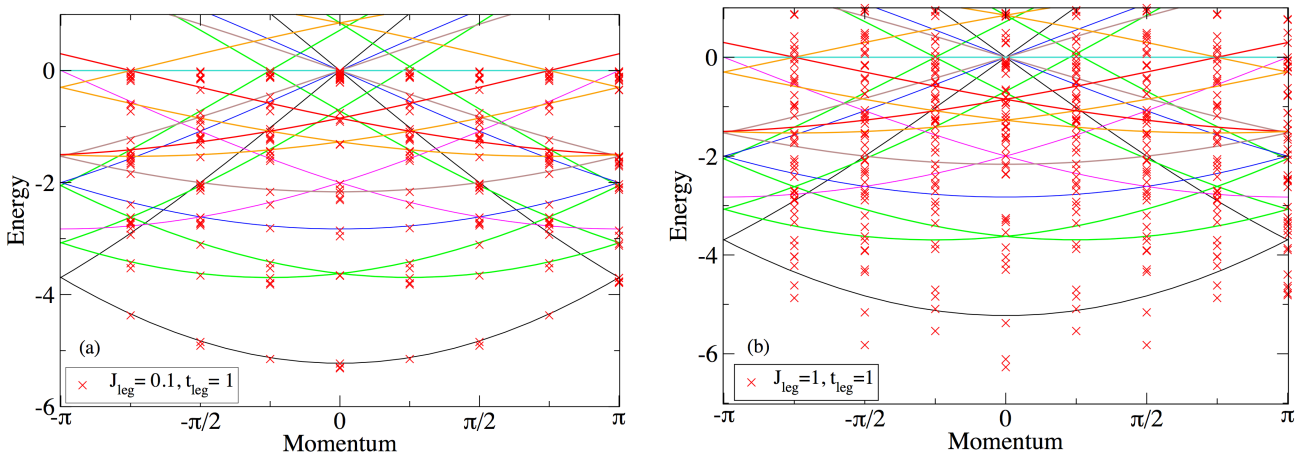

FIG. 15: Splitting of the degenerate levels on switching on different values of $J_{\rm leg}$ on a 2×8 ladder with $\rho = 3/4$ and $J_{\rm rung} = t_{\rm rung} = 1000, t_{\rm leg} = 1, V_{\rm rep} = \infty$. The parabolas show the continuous HCB spectrum relevant for $J_{\rm leg} = 0$ (see Fig. 13) and the red crosses represent the ladder spectrum at (a) $J_{\rm leg} = 0.1$ (b) $J_{\rm leg} = 1$.

showed that the full excitation spectrum of an itinerant anyon chain is made up of two independent contributions originating from the charge degrees of freedom (described in section VI A 2) and the anyon degrees of freedom which are given by a *squeezed* (undoped) anyon chain of length $L_{\rm a} = \tilde{\rho} L$ where $\tilde{\rho}$ is the anyon density on a L site t–J chain of anyons.

We now perform a quantitative comparison of the spectra of the anyonic ladder and its corresponding effective anyonic chain. As the charge spectra match, we focus on the energy difference spectrum (EDS) obtained by subtracting the (supposed) charge excitation component to each state. By construction, the EDS then carries the information about the anyon degrees of freedom. Note that this procedure is only possible at low energy and for small enough $J_{\rm leg}$, *i.e.* when a well defined parabolic charge branch can be assigned unambiguously to the levels we consider. However, even when a large splitting of the energy levels is seen as in Fig. 15(b), we have been able to identify exactly the charge excitations corresponding to the various levels in the low energy spectrum up to an excitation energy of order $5t_{\rm leg}$ and hence obtain the corresponding EDS. The numerical results for the EDS on a 2×8 ladder with anyon density $\rho = 3/4$ for small $J_{\rm leg} = 0.1 t_{\rm leg}$ and intermediate $J_{\rm leg} = t_{\rm leg}$ are shown in Figs. 16(a) and (b) respectively. We find the EDS of the ladder and of the effective chain to be in perfect agreement. The perfect mapping of the two-leg ladder physics to the physics of the chain hence implies straightforwardly that the concept of spin-charge fractionalization is not strictly 1D but also applies to the two-leg anyonic ladder, in contrast to the electronic ladder analog.

Note that the EDS subtracted spectrum must not be confused with the actual energy spectrum of the corresponding squeezed golden chain. In our prescription, subtracting the charge excitations from the full spectrum, we get the spectrum corresponding to the anyon degrees of freedom as a function of the total momentum of the ladder/t–J chain, rather than that of the squeezed golden chain. Thus the spectra shown in Figs. 16(a),(b) are qualitatively different from the golden chain spectra.

B. Three-leg ladder

All results about the t–J phases are summarized in Table III and we provide a short description below.

1. *Density* $\rho < 1/3$

For $\rho < 1/3$, the effective model upon doping the effective golden chain $G_1^{\pm}$ is again a t–J chain ($C_{01}^{\pm}$) independent of the sign of the couplings. Our numerical spectra agree well with the effective model, as shown in Fig. 17 for a 3×6 ladder with $\rho = 5/18$.

Note that, analogously to the case of the two-leg ladder, the mapping to the effective model is exact only in the limit of infinite rung couplings. In Fig. 18, we show the log-log plot for the broadenings Σ for each $E \leq 0$ energy levels in the $K = 0$ sector as a function of the inverse rung couplings for a three-leg ladder. The slope of -1 shows again that, for large but finite rung couplings, there are second order effective processes involving higher

Filling	$J_{\rm rung}$	Phase	$J/J_{\rm leg}$	$t/t_{\rm leg}$	Derivation Eq.	$V/J_{\rm leg}$	Derivation Eq.
$\rho<\frac{1}{3}$	any	$C_{01}^{\pm}$	$\frac{3}{8}$	1	(A49)	—	—
$\frac{1}{3}<\rho<\frac{2}{3}$	>0	$C_{21}^{\pm}$	$\frac{3}{8}$	$\frac{1}{(2+\alpha^2)2\phi}\left[(3+\alpha^2+2\sqrt{2}\alpha)\left(\cos\frac{4\pi}{5}\right)+1\right]$	(A55)	—	—
$\rho>\frac{2}{3}$	>0	$C_{23}^{\pm}$	1	$\frac{1}{2+\alpha^2}\left[\frac{1}{\phi^2}+\frac{\alpha^2}{2\phi}+\frac{\alpha^2}{\phi^3}+1\right]$	(A60)	$-\frac{2}{\phi^2}$	(A29)
$\rho>\frac{2}{3}$	<0	$C_{32}^{\pm}$	$\frac{11}{8\phi^2}$	$\frac{1}{2\phi}-\frac{1}{4}$	(A65)	$\frac{11}{8\phi^3}$	(A26)
any	$>3\phi\lvert t_{\rm rung}\rvert$	PS_{03}	1	$\frac{t_{\rm leg}^2}{E_D^2}(3\phi^{-2}+2\phi^{-3}+\phi^{-2}e^{8\pi i/5})$	(A84)	$-\frac{2}{\phi^2}$	(A29)

TABLE III: Effective couplings for the t–J phases of the three-leg ladder. Here $E_D=(-\phi+\frac{1}{2})J_{\rm rung}+\sqrt{2}t_{\rm rung}+\frac{\sqrt{J_{\rm rung}^2+8t_{\rm rung}^2}}{2}$.

energy states of the rungs.

2. *Density* $1/3<\rho<2/3$ *and* $J_{\rm rung}>0$

In the density regime $1/3<\rho<2/3$, we find an effective t–J model ($C_{21}^{\pm}$) upon doping the $\rho=1/3$ $G_1^{\pm}$ golden chain with heavy holes (increasing the U(1) charge density) or, equivalently, doping the totally gapped $\rho=2/3$ $T_2^{\pm}$ phase with effective light τ particles (reducing the U(1) charge density). Numerical simulations of three-leg ladders in this density regime gives an effective hopping that agrees very well with the analytical estimate.

3. *Density* $\rho>2/3$ *and* $J_{\rm rung}>0$

In the strong antiferromagnetic $J_{\rm rung}>0$ rung coupling limit, increasing the U(1) charge density starting from the $T_2^{\pm}$ gapped chain of heavy holes, introduces super-heavy τ anyons (*i.e.* $|3,\tau\rangle$ states). The system is described by a $C_{23}^{\pm}$ (modified) t–J chain. Unlike in the previous simple t–J chains, the super-heavy τ's experience an effective nearest neighbor *attractive* potential.

4. *Density* $\rho>2/3$ *and* $J_{\rm rung}<0$

For ferromagnetic $J_{\rm rung}<0$ at a density $\rho>2/3$, we map to an effective (modified) t–J chain $C_{32}^{\pm}$ phase of heavy τ's and super-heavy holes. The heavy τ's experience a nearest neighbor *repulsive* potential. Our numerical simulations match very well the analytical estimates.

5. *Phase separation at large* $J_{\rm rung}>0$

In the absence of a rung charging energy $V_{\rm rep}$ an additional phase PS_{03}, that exhibits phase separation, appears for large $J_{\rm rung}>3\phi|t_{\rm rung}|$. The physics of the interacting light holes and super-heavy τ particles is described by an extended 1D t–J–V model that contains the usual couplings of the regular t–J model and, in addition, the nearest neighbor attractive potential V between the super-heavy τ particles. The dominant attraction V leads to phase separation between an empty and a completely filled ladder.

VII. EFFECTIVE MODEL OF HEAVY AND LIGHT FIBONACCI ANYONS

A. The model

We now discuss a new model which appears for strong FM rung couplings on a two-leg ladder with $\rho>1/2$ and a large $V_{\rm rep}$. A similar effective model also describes the three-leg ladder with FM rung couplings and $1/3<\rho<2/3$. When the rung couplings are FM, the fusion of two τ's results in a τ charge. One thus obtains an effective model with two *different* Fibonacci particles, the *heavy* and *light* τ's distinguished by their $U(1)$ charge. For two-leg and three leg ladders, the magnetic interactions (similar to the Golden chain) and the potentials between the different flavors of τ particles are listed in Table IV.

In addition to the magnetic and potential terms one also gets a kinetic process exchanging heavy and light τ's on nearest neighbor rungs. This process is shown schematically in Fig. 19(a),(b) for the microscopic ladder model and the effective chain respectively. Note that, in the t–J chain, with holes and τ's, the hopping process shown in Fig. 1(c) moves the entire particle along with

Width	τ_1	τ_2	$J/J_{\rm leg}$	Eq.	$V/J_{\rm leg}$	Eq.
2	heavy	heavy	$\frac{2}{\phi^2}$	(A12)	$\frac{2}{\phi^3}$	(A11)
2	heavy	light	$-\frac{1}{\phi}$	(A16)	$\frac{1}{\phi}$	(A17)
2	light	light	$\frac{1}{2}$	(A4)	—	—
3	heavy	heavy	$\frac{11}{8\phi^2}$	(A25)	$\frac{11}{8\phi^3}$	(A26)
3	heavy	light	$-\frac{5}{8\phi}$	(A33)	$\frac{5}{8\phi}$	(A34)
3	light	light	$\frac{3}{8}$	(A21)	—	—

TABLE IV: Interactions between heavy and light τ's in two-leg and three-leg ladders. The labels τ_1 and τ_2 indicate the type (heavy or light) of the two interacting particles.

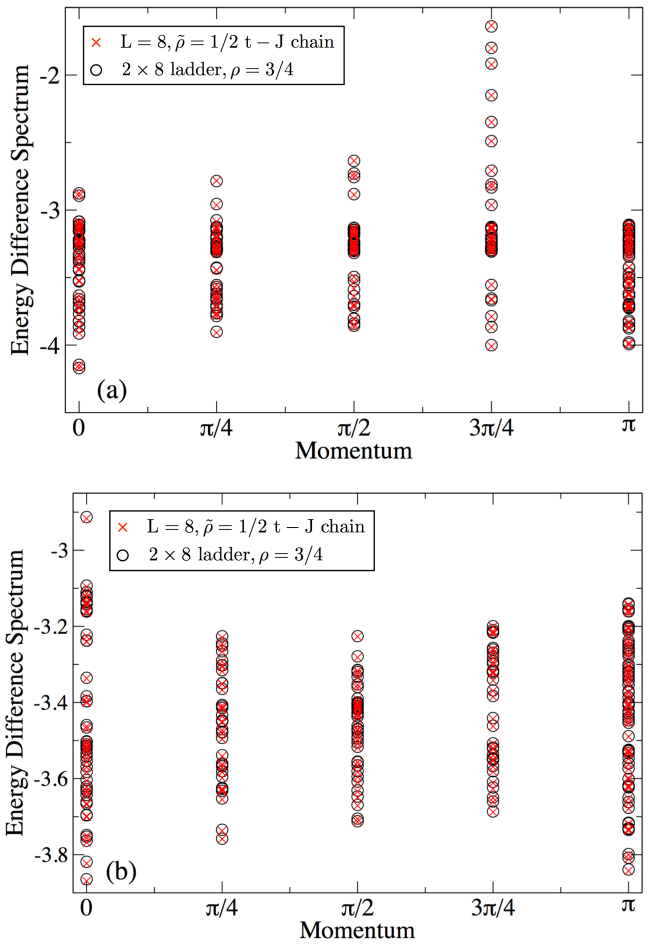

FIG. 16: Comparison of the energy difference spectra, after subtracting the charge contribution to the energy of each state, of a 2×8 ladder, $\rho = 3/4$ with that of the effective t–J chain $L = 8, \tilde{\rho} = 1/2$. The couplings on the ladder are $J_{\rm rung} = t_{\rm rung} = 1000, t_{\rm leg} = 1, V_{\rm rep} = \infty$ and (a) $J_{\rm leg} = 0.1$ and (b) $J_{\rm leg} = 1$.

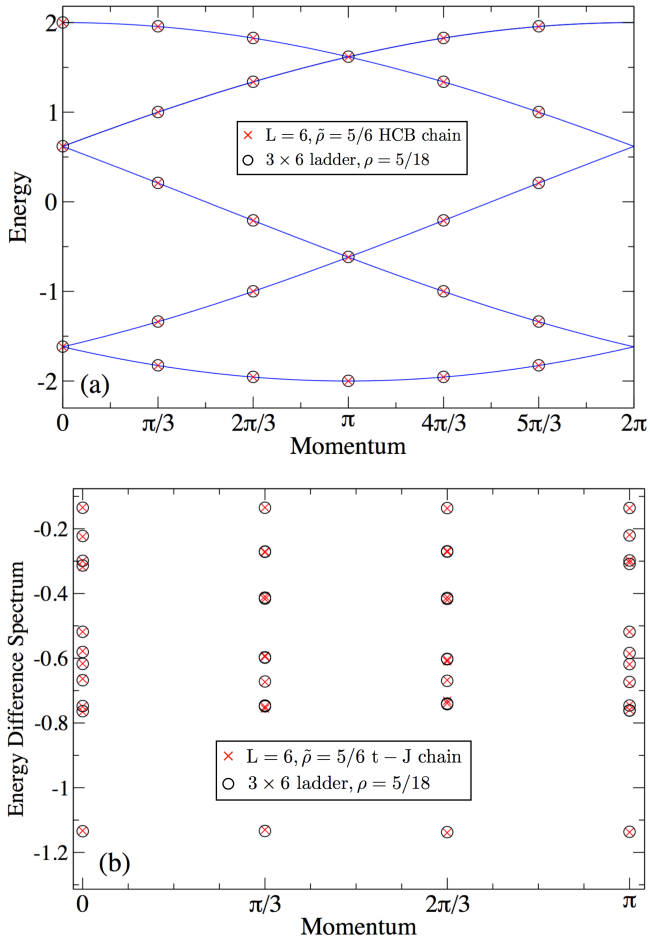

FIG. 17: Three-leg ladder: The black circles denote the spectrum of a 3×6 ladder with $\rho = 5/18$ while the red crosses are for the effective chain with $L = 6$ and $\tilde{\rho} = 5/6$. The couplings on the ladder are $J_{\rm rung} = t_{\rm rung} = 1000, t_{\rm leg} = 1, V_{\rm rep} = \infty$. (a) Charge spectrum at $J_{\rm leg} = 0$. The solid lines denote the HCB spectrum. (b) energy difference spectrum for $J_{\rm leg} = 0.1$.

its charges and spin labels. Whereas now, the scenario is very different, the spin labels mix with each other as the heavy τ's hop over to exchange positions with the light τ's. The effective 1D model (in the basis of Eq. (3)) for the hopping of heavy τ's is described by the Hamiltonian $H_{\rm HL}$ given below

$$H_{\rm HL} = t \begin{bmatrix} 1 & & & & \\ & 0 & & & \\ & & 0 & & \\ & & & \phi^{-2} & \phi^{-3/2} \\ & & & \phi^{-3/2} & \phi^{-1} \end{bmatrix}, \tag{35}$$

where t is the rescaled hopping amplitude. We have found that, for a two-leg ladder, the effective hopping amplitude is

$$t = \cos(3\pi/5) t_{\rm leg}. \tag{36}$$

A proof of this is provided in Eq. (A47).

For a three-leg ladder, the same model applies in the density regime $1/3 < \rho < 2/3$ (see Fig. 12(b) showing the two new low energy states on the rungs) and the hopping amplitude is

$$t = \frac{1}{8}\left[1 + 9\cos(3\pi/5)\right] t_{\rm leg}, \tag{37}$$

as shown in Eq. (A71). Note that there exists a symmetry between the two kinds of τ's *i.e.* the number of heavy and light τ's in the system can be swapped, leaving the physics unchanged. We provide a detailed analytical derivation of this Hamiltonian in Appendix A.

These analytical considerations are found to be in very good agreement with our numerical results for $J_{\rm leg} = 0$. Fig. 20 shows the comparison between the low energy spectra of the effective single chain with heavy and light taus and the ladder model. Note that for $J_{\rm leg} = 0$ there is an exact E → -E symmetry in the spectrum (not

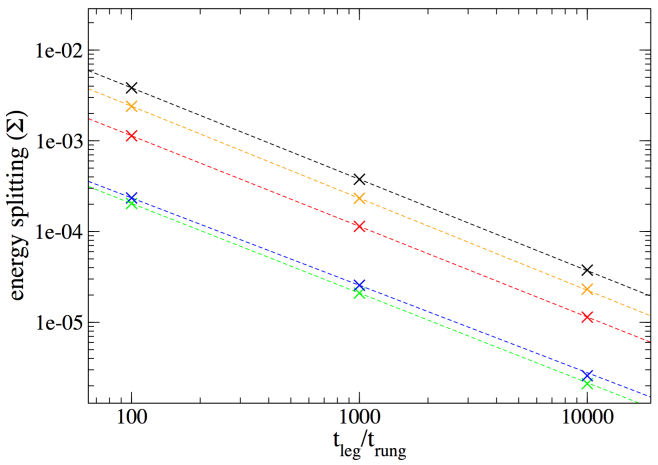

FIG. 18: Energy splittings of all $E \leq 0$ energy levels at $K = 0$ of the 3×6 ladder with $\rho = 5/6$ as a function of $t_{\rm leg}/t_{\rm rung}$. The values of the couplings are $t_{\rm leg} = 1, J_{\rm leg} = 0, V_{\rm rep} = \infty$ and $t_{\rm rung} (= J_{\rm rung})$ takes different values from 100 to 10000.

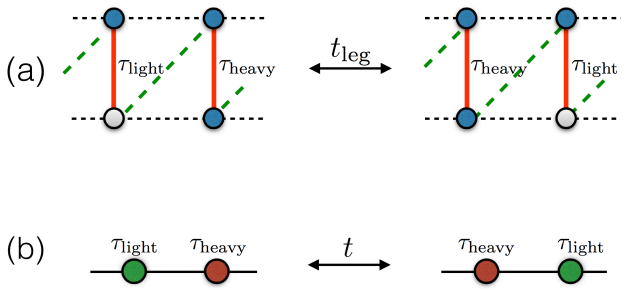

FIG. 19: Hopping of heavy (or equivalently light) τ's. (a) Microscopic ladder model: the blue circles denote τ particles and the white circles are vacant sites on the ladder. (b) The effective chain.

shown here) that emanates from a symmetry of exchanging heavy and light $\tau's$. When there is an odd number of both particle types, the momenta are shifted by π under this exchange.

The 1D model allows us to numerically solve larger systems with smaller finite size corrections. We, however, restrict ourselves to the case $J_{\rm leg} = 0$ when there are no magnetic interactions between τ particles along the leg direction but only a small hopping $t_{\rm leg}$ operates between the rungs since already this simple model raises several open questions.

B. Single particle dispersion

We start with the simplest problem of a single light (heavy) τ moving in a background of $L-1$ τ's of heavy (light) τ. We choose $t = -1$ in order to avoid even-odd chain length effects (although for L even the sign of t is irrelevant). In the spectra shown in Fig. 21 for

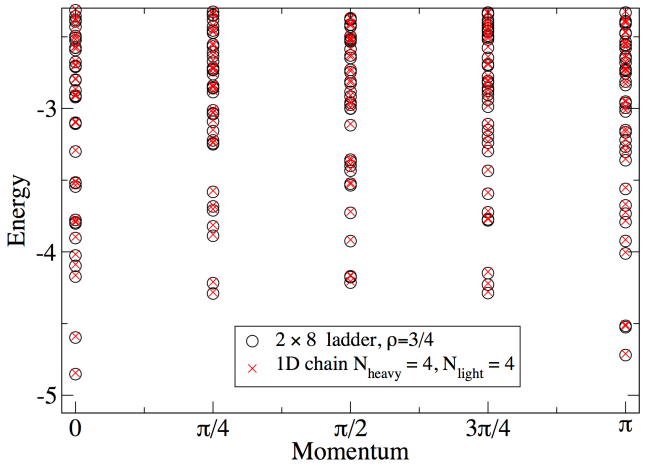

FIG. 20: Low energy spectrum of the two-leg ladder with strong FM rung couplings compared to the 1D heavy and light τ model. The black circles are for a 2×8 ladder and anyon density $\rho = 3/4$, while the red crosses are for the effective chain that it maps to $(L = 8, \tilde{\rho} = 1/2)$. The values of the couplings are $t_{\rm leg} = 1, J_{\rm leg} = 0, V_{\rm rep} = \infty$ and $J_{\rm rung} = -2t_{\rm rung} = -2000$.

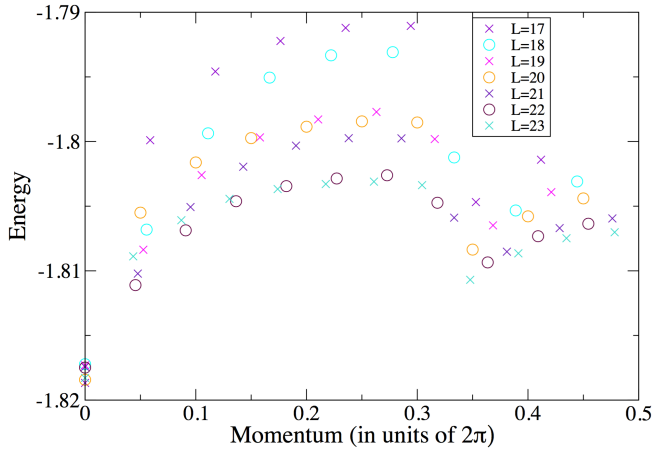

FIG. 21: Energy dispersions of a single heavy (or light) τ amidst $L-1$ light (or heavy) τ's for even (circles) and odd (crosses) length chains, with couplings $t = -1$ and $J = 0$.

several chain lengths we observe that the dispersion minimum is always at $K = 0$ and a local minimum appears around an incommensurate momentum. The bandwidth is about $0.015|t|$, independent of whether we consider a single heavy or light τ.

C. Critical phase at generic fillings

We next consider a finite density $\tilde{\rho}$ of heavy $\tau's$ and a corresponding filling of $1-\tilde{\rho}$ light $\tau's$. Note that due to the symmetry between the heavy and light τ's, densities $\tilde{\rho}$ and $1-\tilde{\rho}$ are equivalent. We expect the same behavior for all densities except for the half-filled case $\tilde{\rho} = 1/2$,

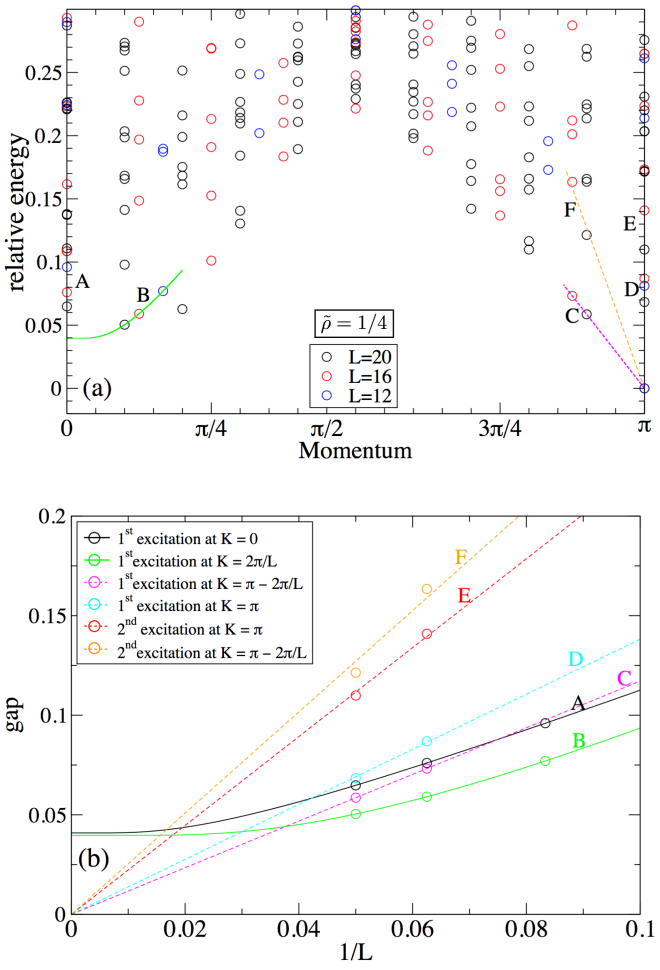

FIG. 22: (a) Spectra for the effective chains for heavy and light $\tau's$ at $\tilde{\rho} = 1/4$ with $t = 1, J = 0$. Note the momenta have been shifted by π for L odd to make all spectra similar and the ground state energy has been subtracted out. The lowest energy levels at momenta 0, $2\pi/L$, $\pi - 2\pi/L$ and π have been tagged as A, B, C and D, respectively. The second excitations at momenta π and $\pi - 2\pi/L$ are labeled by E and F, respectively. (b) Finite-size scaling analysis of the A, B, C, D, E and F energy excitations. Linear (dashed lines) and exponential (full lines) fits are shown around $K = \pi$ and $K = 0$, respectively (see text). The scalings of the B, C and F gaps are also reported in (a).

which we shall consider separately in the next section. For simplicity we thus choose $\tilde{\rho} = 1/4$ since it allows us to perform a finite size analysis using three different chain lengths $L = 12$, 16, 20. The corresponding spectra are shown in Fig. 22(a).

One-dimensional gapless systems are often described by a CFT and their lowest energy levels are then given by

$$E(L) = e_T L + \frac{2\pi v}{L}(-\frac{c}{12} + h_L + h_R). \qquad (38)$$

where c is the central charge and h_L, h_R are the scaling dimensions of the 'primary fields' of the CFT. The (thermodynamic) ground state energy per site e_T and the velocity v are non-universal constants. The finite size ground state energy $E_0(L)$ corresponds to $h_L = h_R = 0$.

To test the CFT prediction, we performed a finite-size scaling analysis of the first few energy gaps vs $1/L$. As shown in Fig. 22(b), we observe that the gaps around $K = \pi$ show a linear scaling with $1/L$, suggesting gapless modes. This behavior is, in principle, consistent with the CFT scaling of Eq. (38). However, at this point, we could not identify the CFT that describes our model, being limited in Lanczos exact diagonalizations to system sizes of less then twenty sites. Using the density matrix renormalization group (DMRG) might help to obtain the central charge, but is left for future studies.

The energy spectrum around $K = 0$ shows a different behavior: as shown in Fig. 22(b), the finite size gaps of the first excited states at momentum $K = 0$ and $K = 2\pi/L$ could be fitted as $\Delta(L) = \Delta(\infty) + C/L \exp(-L/\xi)$, where $\Delta(\infty) \simeq 0.04$ is a finite energy gap and $\xi > 10$ is a correlation length. This suggests that, at density $\tilde{\rho} = 1/4$, the energy spectrum shows both a gapless mode with linear disperson, described by a CFT, and additional gapped modes.

D. Possible topological gapped phase at $\tilde{\rho} = 1/2$

Next we consider the density $\tilde{\rho} = 1/2$ where there is an equal number of heavy and light $\tau's$. We simulated chains with lengths $L = 14$, 16, 18, and 20 and show these spectra in Fig. 23(a), revealing low energy excitations at momenta $K = 0$ and $K = \pi$. Performing a finite size scaling analysis on the low lying states using system sizes L ranging from 14 to 20 sites, as shown in Fig. 23(b) we find that an exponential form like $\Delta(L) = \Delta(\infty) + C/L \exp(-L/\xi)$ provides reasonably good fits of the data. These fits suggest that three of the gaps extrapolate to zero and the next higher energy excitations extrapolate to a finite value $\Delta(\infty) \sim 0.05$. Note however, that the correlation lengths extracted from the fits are of the order of the system size so that our extrapolations have to be taken with caution. However, if correct, our findings would indicate a topological gapped phase with a four-fold degenerate ground state, although dimerization is not excluded (since ground state momenta are both 0 and π). In any case, we believe half-filling is a special case and very different from the other density regimes we considered. This behavior is also notably different from the golden chains which are known to be gapless for both FM and AFM leg couplings.

VIII. CONCLUSIONS AND OUTLOOK

The possible realization of Fibonacci anyons in experiments and their potential application to topological quantum computing continues to fascinate many physicists to work with such systems. In this article, we have

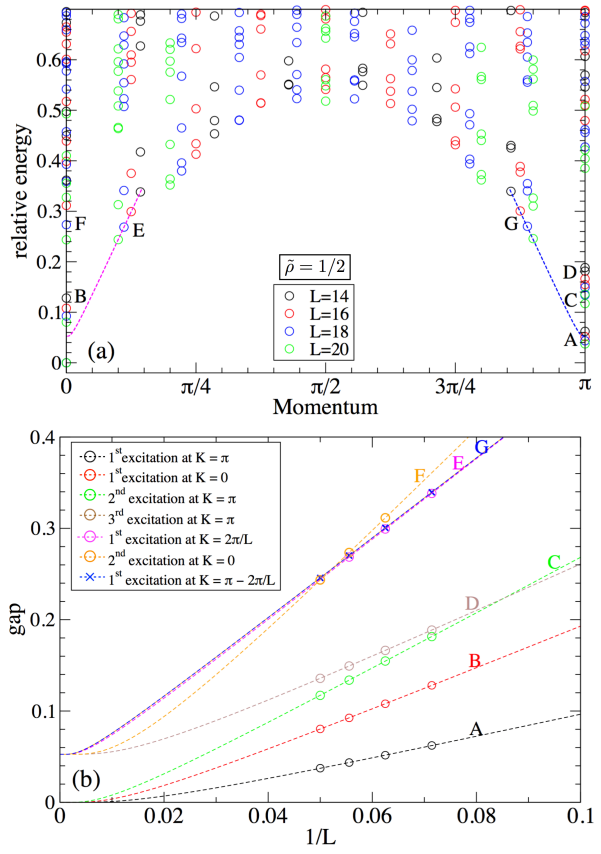

FIG. 23: (a) Spectra of the chains of heavy and light τ's of different sizes at $\tilde{\rho} = 1/2$ and $t = 1, J = 0$. The ground state energy has been subtracted out and the momenta are shifted by π for odd number of particles of each type so as to get the same zero ground state momentum in all cases. The lowest energy levels at momenta 0, $2\pi/L$, $\pi - 2\pi/L$ and π have been tagged as B, E, G, A, respectively. The second excitations at momenta 0 and π are labeled by F and C, respectively. The third excitation at momentum π is labeled by D. (b) Finite-size scaling analysis of the energy gaps of (a) vs $1/L$ (see text). The scalings of the E and G gaps are also reported in (a).

addressed some questions on the physics of itinerant interacting Fibonacci anyons in two dimensions. We have studied two and three-leg ladders of doped Fibonacci anyons and mapped out their phase diagrams. Motivated by the construction of this model that forms an anyonic generalization of the fermionic $t - J$ model, we employed a similar scheme of analysis by working in the strong rung coupling limit. We start off with the limit of isolated rungs and then couple them weakly by switching on small interactions along the leg direction. In this limit we find several different phases: totally gapped phases, paired phases described by hard core bosons, golden chain phases, $t-J$ phases that carry τ anyons and trivial particles and lastly the heavy and light τ phase that carries two flavors of Fibonacci anyons. The bosonic phases as well as the anyonic phases of the golden chain/ladder and the $t-J$ phases have been studied before. However, in addition to the existing known phases, our study of doped Fibonacci ladders has revealed a new heavy-light τ model that can possibly realize a topological gapped stated for some special filling, whereas a critical phase otherwise. For each of the above-mentioned phases we have analytically constructed effective low energy models and shown that they indeed corroborate our numerical simulations.

An important point established in this article is that we can map 2D doped Fibonacci ladders to effective 1D models of Fibonacci anyons, some of which have been well studied in the past. By introducing the idea of an energy difference spectrum and building on our mapping to effective 1D models, we have shown that the phenomenon of spin-charge separation continues to hold even in two-dimensions on ladders of non-Abelian anyons.

The mapping to effective 1D models would allow these ladder models of interacting anyons to be easily simulated numerically by efficient 1D algorithms such as DMRG which pave the way for other potential studies that could be carried out on these systems. There are still some questions for the heavy-light τ model that remain unanswered, which would certainly give us more insight into the physics of the model. In particular, we have identified gapless modes for (certain fillings of) the heavy-light τ model, but are restricted by means of computational power to ascertain the CFT that governs this model. Our exact diagonalization simulations do not allow us to probe very large system sizes, hence extrapolate the behaviour of the system to the thermodynamic limit. This open question could perhaps be tackled by means of efficient 1D computational methods.

Acknowledgments

M.S. and D.P. acknowledge the support from NQPTP Grant No. ANR-0406-01 from the French Research Council (ANR) and the HPC resources of CALMIP (Toulouse) for CPU time under project P1231. M.T. acknowledges hospitality of the Aspen Center for Physics, supported by NSF grant 1066293.

Appendix A: Effective models

In this Appendix we explain the derivation of the effective models. We perturbatively derive the nearest neighbor couplings of the effective 1D models assuming large rung couplings and small leg couplings: $|J_{\rm rung}|, |t_{\rm rung}| \gg |J_{\rm leg}|, |t_{\rm leg}|$.

1. Magnetic and Potential Interactions

Magnetic interactions will only be present in effective models if two neighboring sites each have a total anyonic τ charge. A rung state with a total anyonic τ charge can

j \ $U(1)$	0	1	2	3
0	light	×	heavy	super heavy
1	×	light	heavy	super heavy

TABLE V: The various rung states classified according to their U(1) charge (columns) and topological charge (lines). $j = 0$ ($j = 1$) corresponds to holes (τ particles). The possible magnetic interactions (in the present models) are indicated by pink arrows and the green arrows represent the possible kinetic terms arising in first-order perturbation in $t_{\rm leg}$. The leading kinetic and potential interactions can also arise only in second or third-order in $t_{\rm leg}$, marked by blue and orange arrows respectively.

have one (light τ), two (heavy τ) or three (super heavy τ) τ particles on the rung, as shown in Table V. The possible magnetic interactions are marked by pink arrows. Below we investigate all possible combinations for two neighboring rungs in two-leg and three-leg ladders, respectively and compute the effective interactions from first-order perturbation in $J_{\rm leg}$.

a. *Two-leg ladder*

For the two-leg ladder the rungs have to be in the light τ state

$$|1^{\pm},\tau\rangle = \frac{1}{\sqrt{2}}\big(|1^{U},\tau\rangle \pm |1^{L},\tau\rangle\big) \equiv \frac{|U\rangle \pm |L\rangle}{\sqrt{2}}, \qquad \text{(A1)}$$

or in the heavy τ state $|2,\tau\rangle$, where we introduced short hand notations $|U\rangle$ and $|L\rangle$ for an anyon on the upper or lower site of a rung, respectively. We review three possible cases below.

Light τ − light τ : We first evaluate the matrix element $\langle\psi|H^{\rm leg}_{\rm magn}|\psi\rangle$ of the state

$$\begin{aligned} |\psi\rangle &= |1^{\pm},\tau\rangle \otimes |1^{\pm},\tau\rangle \\ &= \frac{1}{2}(|UU\rangle \pm |LU\rangle \pm |UL\rangle + |LL\rangle), \end{aligned} \qquad \text{(A2)}$$

where $H^{\rm leg}_{\rm magn}$ is the (part of the) Hamiltonian that describes the magnetic interaction between two anyons once they are nearest neighbors along a leg of the ladder (see main text).

The only non-vanishing matrix elements for the magnetic interaction in the effective model arise when the two anyons are on the same leg of the ladder. Thus, we have

$$\begin{aligned} \langle\psi|H^{\rm leg}_{\rm magn}|\psi\rangle &= \frac{1}{4}(\langle UU|H^{\rm leg}_{\rm magn}|UU\rangle + \langle LL|H^{\rm leg}_{\rm magn}|LL\rangle) \\ &= \frac{1}{2}\langle UU|H^{\rm leg}_{\rm magn}|UU\rangle. \end{aligned} \qquad \text{(A3)}$$

The second step follows since the contributions from magnetic interactions on the upper and lower legs of the ladder are equal in magnitude. It follows immediately that the effective magnetic interaction is half the bare interaction:

$$J = \frac{1}{2}J_{\rm leg}. \qquad \text{(A4)}$$

Heavy τ − heavy τ : Let us now consider the case where both rungs are in the heavy τ state. The state $|\psi\rangle$ is now defined by

$$|\psi\rangle = |2,\tau\rangle \otimes |2,\tau\rangle\,. \qquad \text{(A5)}$$

We calculate the matrix element $\langle\psi|H^{\rm leg}_{\rm magn}|\psi\rangle$ for this state to obtain

$$\begin{aligned} \langle\psi|H^{\rm leg}_{\rm magn}|\psi\rangle &= (\langle UU|H^{\rm leg}_{\rm magn}|UU\rangle + \langle LL|H^{\rm leg}_{\rm magn}|LL\rangle) \\ &= 2\langle UU|H^{\rm leg}_{\rm magn}|UU\rangle\,, \end{aligned} \qquad \text{(A6)}$$

where the second steps follows since both the terms have the same contribution.

To evaluate the contribution of such a term, we need to calculate explicitly the matrix elements for all bond labels. The bond labels belong to the set $\mathcal{S}$ defined in Eq. (3), which we rewrite here for convenience

$$\mathcal{S} = \{|\mathbf{1}\tau\mathbf{1}\rangle, |\mathbf{1}\tau\tau\rangle, |\tau\tau\mathbf{1}\rangle, |\tau\mathbf{1}\tau\rangle, |\tau\tau\tau\rangle\}. \qquad \text{(A7)}$$

We denote the initial quantum state (including site and bond labels) as:

$$|\Psi_\alpha\rangle = \big|\psi;\xi_\alpha\big\rangle, \qquad \text{(A8)}$$

where $|\xi_\alpha\rangle \in \mathcal{S}$. The final states after the magnetic process are given by :

$$|\Psi_\beta\rangle = \big|\psi;\xi_\beta\big\rangle, \qquad \text{(A9)}$$

where $|\xi_\beta\rangle \in \mathcal{S}$.

Then, the matrix elements for this process in the basis $\mathcal{S}$ are given by:

$$H^{\rm leg}_{\rm magn} = -J_{\rm leg}\begin{bmatrix} \phi^{-1} & & & & & \\ & \phi^{-3} & & & & \\ & & \phi^{-3} & & & \\ & & & \phi^{-2} & \phi^{-7/2} & \\ & & & \phi^{-7/2} & \phi^{-2}+\phi^{-5} & \end{bmatrix}. \qquad \text{(A10)}$$

This effective Hamiltonian is proportional to the golden chain Hamiltonian (upto an overall shift) and the contribution to the effective coupling on each leg is $\phi^{-2}J_{\rm leg}$. Thus, the effective potential between the two heavy τ's is given by

$$V = 2\phi^{-3}J_{\rm leg}, \qquad \text{(A11)}$$

and the effective magnetic interaction for the entire process obtained by combining contributions from both the legs (see Eq. (A6)), is thus given by

$$J = 2\phi^{-2}J_{\rm leg}\,. \qquad \text{(A12)}$$

Light τ − heavy τ : Finally, we consider the case where we have a heavy τ and light τ on neighboring rungs. The state $|\psi\rangle$ is now defined as

$$|\psi\rangle \;=\; |1^{\pm},\tau\rangle \otimes |2,\tau\rangle\,. \tag{A13}$$

We calculate the matrix element $\langle\psi|H^{\rm leg}_{\rm magn}|\psi\rangle$ for this state to obtain

$$\begin{aligned}\langle\psi|H^{\rm leg}_{\rm magn}|\psi\rangle \;&=\; \frac{1}{2}(\langle UU|H^{\rm leg}_{\rm magn}|UU\rangle + \langle LL|H^{\rm leg}_{\rm magn}|LL\rangle)\\ &=\; \langle UU|H^{\rm leg}_{\rm magn}|UU\rangle\,,\end{aligned} \tag{A14}$$

where the second steps follows since both the terms have the same contribution. As before we denote the initial and final states as defined in Eq. (A8) and Eq. (A9) respectively. Then, the matrix elements for this process in the basis $\mathcal{S}$ are given by:

$$H^{\rm leg}_{\rm magn} = -J_{\rm leg}\begin{bmatrix} 0 & & & & \\ & \phi^{-1} & & & \\ & & \phi^{-1} & & \\ & & & \phi^{-2} & -\phi^{-5/2} \\ & & & -\phi^{-5/2} & \phi^{-3} \end{bmatrix}. \tag{A15}$$

This Hamiltonian matrix is equivalent to the golden chain Hamiltonian with the effective coupling

$$J = -\phi^{-1}J_{\rm leg} \tag{A16}$$

and an effective potential

$$V = \phi^{-1}J_{\rm leg} \tag{A17}$$

b. Three-leg ladder

For three legs, a rung has a total anyonic τ charge if it is in one of the $|1^{\pm},\tau\rangle$ (light), $|2^{\pm},\tau\rangle$ (heavy) or $|3,\tau\rangle$ (super heavy) state. Below we consider all possible cases for neighboring rungs both with a total anyonic τ charge.

Light τ − light τ : We first assume that the two rungs are both in the state

$$\begin{aligned}|1^{\pm},\tau\rangle \;&=\; \frac{1}{2}\big(|1^{U},\tau\rangle + |1^{L},\tau\rangle \pm \sqrt{2}|1^{M},\tau\rangle\big)\\ &=\; \frac{1}{2}|L\rangle \pm \frac{1}{\sqrt{2}}|M\rangle + \frac{1}{2}|U\rangle,\end{aligned} \tag{A18}$$

where the states $|L\rangle, |M\rangle, |U\rangle$ denote the position of the anyon on the lower, middle or upper leg respectively, and $\pm$ depends on the sign of $t_{\rm rung}$. As above we calculate the matrix element for the state

$$|\psi\rangle = |1^{\pm},\tau\rangle \otimes |1^{\pm},\tau\rangle \tag{A19}$$

and obtain

$$\begin{aligned}\langle\psi|H^{\rm leg}_{\rm magn}|\psi\rangle \;&=\; \frac{1}{16}\big(\langle UU|H^{\rm leg}_{\rm magn}|UU\rangle\\ &+\; \langle LL|H^{\rm leg}_{\rm magn}|LL\rangle\\ &+\; \frac{1}{4}\langle MM|H^{\rm leg}_{\rm magn}|MM\rangle\big)\\ &=\; \frac{3}{8}\langle UU|H^{\rm leg}_{\rm magn}|UU\rangle,\end{aligned} \tag{A20}$$

resulting in an effective coupling

$$J = \frac{3}{8}J_{\rm leg}. \tag{A21}$$

Heavy τ − heavy τ : Let us now assume the effective τ's on the rungs are in the heavy τ state

$$\begin{aligned}|2^{\pm},\tau\rangle \;&=\; \frac{1}{2}\big(|1^{U,M},\tau\rangle + |1^{M,L},\tau\rangle \pm \sqrt{2}|1^{U,L},\tau\rangle\big)\\ &\equiv\; \frac{1}{2}\big(|UM\rangle + |ML\rangle \pm \sqrt{2}|UL\rangle\big),\end{aligned} \tag{A22}$$

where we have used the short hand notation $|AB\rangle$ denoting that the τ lies on the leg A and B and the net fusion channel outcome being a τ is implicit.

As above we calculate the matrix element for the state

$$\begin{aligned}|\psi\rangle \;&=\; |2^{\pm},\tau\rangle \otimes |2^{\pm},\tau\rangle\\ &=\; \frac{1}{4}\big(|UM,UM\rangle + |UM,ML\rangle + \sqrt{2}|UM,UL\rangle\\ &+\; |ML,UM\rangle + |ML,ML\rangle + \sqrt{2}|ML,UL\rangle\\ &+\; \sqrt{2}|UL,UM\rangle + \sqrt{2}|UL,ML\rangle + 2|UL,UL\rangle\big)\end{aligned} \tag{A23}$$

and obtain

$$\begin{aligned}\langle\psi|H^{\rm leg}_{\rm magn}|\psi\rangle \;&=\; \frac{1}{16}\big(\langle UM,UM|H^{\rm leg}_{\rm magn}|UM,UM\rangle\\ &+\; \langle ML,ML|H^{\rm leg}_{\rm magn}|ML,ML\rangle\\ &+\; 2\langle UL,UL|H^{\rm leg}_{\rm magn}|UL,UL\rangle\\ &+\; \langle UM,ML|H^{\rm leg}_{\rm magn}|UM,ML\rangle\\ &+\; \sqrt{2}\langle UM,UL|H^{\rm leg}_{\rm magn}|UM,UL\rangle\\ &+\; \langle ML,UM|H^{\rm leg}_{\rm magn}|ML,UM\rangle\\ &+\; \sqrt{2}\langle ML,UL|H^{\rm leg}_{\rm magn}|ML,UL\rangle\\ &+\; \sqrt{2}\langle UL,UM|H^{\rm leg}_{\rm magn}|UL,UM\rangle\\ &+\; \sqrt{2}\langle UL,ML|H^{\rm leg}_{\rm magn}|UL,ML\rangle\big)\,.\end{aligned} \tag{A24}$$

The first three terms have two magnetic interactions each along the leg direction while all the others have only one. Moreover all these magnetic interactions are equal in magnitude, the contribution of a single term giving the effective coupling $J = \phi^{-2}J_{\rm leg}$ (see Eq. (A12)). Taking into account the contributions from all the terms, it follows immediately that the effectively magnetic coupling is

$$J = \frac{11}{8}\phi^{-2}J_{\rm leg} \tag{A25}$$

and the effective potential is given by

$$V = \frac{11}{8}\phi^{-3} J_{\rm leg}\,. \tag{A26}$$

Super-heavy τ − super-heavy τ : Let us now assume the states on the rungs with total anyonic charge τ are both given by $|3,\tau\rangle$ (super-heavy τ's). Then, we calculate the matrix element for the state

$$|\psi\rangle = |3,\tau\rangle \otimes |3,\tau\rangle \tag{A27}$$

and obtain

$$\begin{aligned}\langle\psi|H^{\rm leg}_{\rm magn}|\psi\rangle &= \big(\langle UU|H^{\rm leg}_{\rm magn}|UU\rangle \\ &+ \langle LL|H^{\rm leg}_{\rm magn}|LL\rangle \\ &+ \langle MM|H^{\rm leg}_{\rm magn}|MM\rangle\big)\,. \end{aligned}\tag{A28}$$

Magnetic interactions on the upper and middle leg contribute to a potential in the effective Hamiltonian given by

$$V = -2\phi^{-2} J_{\rm leg}\,, \tag{A29}$$

while the magnetic process on the lower leg results in an effective magnetic coupling given by

$$J = J_{\rm leg}\,. \tag{A30}$$

Light τ − heavy τ : Finally, we consider the case when the two τ's on the neighboring rungs are in the $|1^{\pm},\tau\rangle$ and the $|2^{\pm},\tau\rangle$ states. The state $|\psi\rangle$ is now given by

$$\begin{aligned}|\psi\rangle &= |2^{\pm},\tau\rangle \otimes |1^{\pm},\tau\rangle \\ &= \frac{1}{2}\big(|UM\rangle + |ML\rangle + \sqrt{2}|UL\rangle\big) \\ &\otimes \frac{1}{2}\big(|U\rangle + |L\rangle + \sqrt{2}|M\rangle\big) \\ &= |UM,U\rangle + |UM,L\rangle + \sqrt{2}|UM,M\rangle \\ &+ |ML,U\rangle + |ML,M\rangle + \sqrt{2}|ML,M\rangle \\ &+ \sqrt{2}|UL,U\rangle + \sqrt{2}|UL,L\rangle + 2|UL,M\rangle\,. \end{aligned}\tag{A31}$$

As before we calculate the matrix element

$$\begin{aligned}\langle\psi|H^{\rm leg}_{\rm magn}|\psi\rangle &= \frac{1}{16}\big(\langle UM,U|H^{\rm leg}_{\rm magn}|UM,U\rangle \\ &+ 2\langle UM,M|H^{\rm leg}_{\rm magn}|UM,M\rangle \\ &+ \langle ML,L|H^{\rm leg}_{\rm magn}|ML,L\rangle \\ &+ 2\langle ML,M|H^{\rm leg}_{\rm magn}|ML,M\rangle \\ &+ 2\langle UL,U|H^{\rm leg}_{\rm magn}|UL,U\rangle \\ &+ 2\langle UL,L|H^{\rm leg}_{\rm magn}|UL,L\rangle\big)\,. \end{aligned}\tag{A32}$$

The contributions of each of these terms to the effective coupling is $(-\phi^{-1})J_{\rm leg}$ (see Eq. (A16)), thus the net effective coupling for this magnetic process is given by

$$J = -\frac{5}{8\phi} J_{\rm leg} \tag{A33}$$

and the effective potential is

$$V = \frac{5}{8\phi} J_{\rm leg} \tag{A34}$$

2. Kinetic terms

Whenever the total U(1) charges of the two neighboring rung states differ by ± 1, a hopping process occurs in first order in $t_{\rm leg}$. It is the case for a charge-1 (light) τ and a charge-0 (light) or charge-2 (heavy) hole, a charge-1 (light) τ and a charge-2 (heavy) τ, a charge-2 (heavy) hole and a charge-3 (super heavy) τ, a charge-2 (heavy) τ and a charge-3 (super heavy) hole. All these are marked schematically by green arrows in Table. V. Below we investigate all these possibilities in two leg and three leg ladders, respectively.

a. Two-leg ladder

Let us first evaluate the effective hopping in a two-leg ladder arising when there is a τ particle in the state $|1^{\pm},\tau\rangle$ and an effective hole in either the empty $|e\rangle = |0,\mathbf{1}\rangle$ (case 1) or the fully occupied $|f\rangle = |2,\mathbf{1}\rangle$ (case 2) rung state on adjacent rungs.

Light hole − light τ : First, we need to evaluate the matrix element $\langle\Psi_1|H^{\rm leg}_{\rm kin}|\Psi_2\rangle$ between the two states

$$|\Psi_1\rangle = |1^{\pm},\tau\rangle \otimes |e\rangle \equiv \frac{|Ue\rangle \pm |Le\rangle}{\sqrt{2}} \tag{A35}$$

and

$$|\Psi_2\rangle = |e\rangle \otimes |1^{\pm},\tau\rangle \equiv \frac{|eU\rangle \pm |eL\rangle}{\sqrt{2}}, \tag{A36}$$

where $H^{\rm leg}_{\rm kin}$ is the kinetic part of the ladder Hamiltonian living on the legs (see main text). Similar to the case of magnetic interactions one gets a factor 1/2 and obtains for the effective hopping

$$t = \frac{1}{2} t_{\rm leg}. \tag{A37}$$

Heavy hole − light τ : Next, one evaluates the matrix element between the states

$$|\Psi_1\rangle = |1^{\pm},\tau\rangle \otimes |f\rangle \equiv \frac{|Uf\rangle \pm |Lf\rangle}{\sqrt{2}} \tag{A38}$$

and

$$|\Psi_2\rangle = |f\rangle \otimes |1^{\pm},\tau\rangle \equiv \frac{|fU\rangle \pm |fL\rangle}{\sqrt{2}}\,. \tag{A39}$$

The matrix elements are written explicity as

$$\langle\Psi_2|H^{\rm leg}_{\rm kin}|\Psi_1\rangle = \frac{1}{2}\langle fU|H^{\rm leg}_{\rm kin}|Uf\rangle + \frac{1}{2}\langle fL|H^{\rm leg}_{\rm kin}|Lf\rangle\,. \tag{A40}$$

The derivation is identical but involves two non-trivial braids. The contributions from the hopping on the two legs are thus given by

$$\begin{aligned}\langle fU|H^{\rm leg}_{\rm kin}|Uf\rangle &= e^{4\pi i/5}\phi^{-1}t_{\rm leg}\langle \mathbf{1}\tau|h_{\rm kin}|\tau\mathbf{1}\rangle,\\ \langle fL|H^{\rm leg}_{\rm kin}|Lf\rangle &= e^{-4\pi i/5}\phi^{-1}t_{\rm leg}\langle \mathbf{1}\tau|h_{\rm kin}|\tau\mathbf{1}\rangle.\end{aligned} \tag{A41}$$

Adding both the terms we get an overall -1 factor, compared to the previous case:

$$t = -\frac{1}{2}t_{\rm leg}. \tag{A42}$$

Light τ – heavy τ : Finally, let us consider two nearest neighbor rungs, one carrying a heavy τ and the other with a light τ. Here, the bond labels belong to the set $\mathcal{S}$ defined in Eq. (A7). We denote the 'initial' quantum state (including site and bond labels) with a light (heavy) τ on the first (second) rung as:

$$|\Psi_{i,\alpha}\rangle = \big|1_l 2_h; \xi_\alpha\rangle, \tag{A43}$$

where i stands for initial and $|\xi_\alpha\rangle \in \mathcal{S}$. The 'final' states after the hopping process are given by :

$$|\Psi_{f,\beta}\rangle = \big|1_h 2_l; \xi_\beta\rangle, \tag{A44}$$

where f is for final and $|\xi_\beta\rangle \in \mathcal{S}$. One needs to compute all matrix elements $\big\langle \Psi_\beta|H^{\rm leg}_{\rm kin}|\Psi_\alpha\big\rangle$. The matrix elements for the hopping of a heavy and a light τ on the lower leg of the ladder are found to be:

$$\begin{aligned}\big\langle 1_h 2_l; \mathbf{1}\tau\mathbf{1}|H^{\rm leg}_{\rm kin}|1_l 2_h; \mathbf{1}\tau\mathbf{1}\big\rangle &= t_{\rm leg}e^{-3\pi i/5}\langle \mathbf{1}\tau|h_{\rm kin}|\tau\mathbf{1}\rangle,\\ \big\langle 1_h 2_l; \mathbf{1}\tau\tau|H^{\rm leg}_{\rm kin}|1_l 2_h; \mathbf{1}\tau\tau\big\rangle &= -t_{\rm leg}e^{-3\pi i/5}\phi^{-1}\langle \mathbf{1}\tau|h_{\rm kin}|\tau\mathbf{1}\rangle,\\ \big\langle 1_h 2_l; \tau\tau\mathbf{1}|H^{\rm leg}_{\rm kin}|1_l 2_h; \tau\tau\mathbf{1}\big\rangle &= -t_{\rm leg}e^{-3\pi i/5}\phi^{-1}\langle \mathbf{1}\tau|h_{\rm kin}|\tau\mathbf{1}\rangle,\\ \big\langle 1_h 2_l; \tau\mathbf{1}\tau|H^{\rm leg}_{\rm kin}|1_l 2_h; \tau\tau\tau\big\rangle &= \big\langle 1_h 2_l; \tau\tau\tau|H^{\rm leg}_{\rm kin}|1_l 2_h; \tau\mathbf{1}\tau\big\rangle = t_{\rm leg}e^{-3\pi i/5}\phi^{-1/2}\langle \mathbf{1}\tau|h_{\rm kin}|\tau\mathbf{1}\rangle,\\ \big\langle 1_h 2_l; \tau\tau\tau|H^{\rm leg}_{\rm kin}|1_l 2_h; \tau\tau\tau\big\rangle &= t_{\rm leg}e^{-3\pi i/5}\phi^{-2}\langle \mathbf{1}\tau|h_{\rm kin}|\tau\mathbf{1}\rangle.\end{aligned} \tag{A45}$$

The matrix elements for hopping on the other leg remain the same except for the direction of the braid being reversed, *i.e.* all phase factors $e^{-3\pi i/5} \to e^{3\pi i/5}$. As we sum up contributions from both the legs, the phase factors add up and the entire matrix (in the basis (A7)) is written as :

$$H_{\rm eff} = t\begin{bmatrix} 1 & & & & & \\ & -\phi^{-1} & & & & \\ & & -\phi^{-1} & & & \\ & & & 0 & \phi^{-1/2} & \\ & & & \phi^{-1/2} & \phi^{-2} & \end{bmatrix}, \tag{A46}$$

where the effective hopping amplitude is

$$t = \big(\cos(3\pi/5)\big)t_{\rm leg}. \tag{A47}$$

A characteristic feature of this effective hopping Hamiltonian is that it mixes the spin labels. This is remarkably different from the simple hopping process between a hole and a τ. In the text, we have quoted the effective Hamiltonian matrix for this process as $H_{\rm HL}$ described in Eq. (35), which is related to $H_{\rm eff}$ by rescaling it such that the 2×2 block has eigenvalues 0 and 1. More precisely, $H_{\rm HL} = aH_{\rm eff} + b\mathbb{I}$ with $a = \phi^{-1}$ and $b = \phi^{-2}$ (where $\mathbb{I}$ is the identity matrix).

b. *Three-leg ladder*

For a three-leg ladder, we can derive the relevant matrix elements in a similar way.

Light hole – light τ : Let us start with the simplest case and compute the matrix element $\big\langle \Psi_1|H^{\rm leg}_{\rm kin}|\Psi_2\big\rangle$ where $|\Psi_1\rangle = |s\rangle\otimes|e\rangle$, $|\Psi_2\rangle = |e\rangle\otimes|s\rangle$, $|s\rangle \equiv |1^{\pm}, \tau\rangle$ is defined in (A18) and $|e\rangle$ is the empty rung. Using obvious notations,

$$\begin{aligned}\big\langle \Psi_1|H^{\rm leg}_{\rm kin}|\Psi_2\big\rangle &= \frac{1}{4}\big(\langle eU|H^{\rm leg}_{\rm kin}|Ue\rangle\\ &+ 2\big\langle eM|H^{\rm leg}_{\rm kin}|Me\big\rangle\\ &+ \big\langle eL|H^{\rm leg}_{\rm kin}|Le\rangle\big)\\ &= \big\langle eU|H^{\rm leg}_{\rm kin}|Ue\rangle,\end{aligned} \tag{A48}$$

Since all the F-moves are trivial because of the holes on the rungs and there would be no phase factors due to the braidings either, we get the effective hopping:

$$t = t_{\rm leg}. \tag{A49}$$

Heavy hole – light τ : The calculation is slightly more involved when the effective effective hole state $|d\rangle$ involves two τ anyons on the rung,

$$|d\rangle = \frac{1}{\sqrt{2+\alpha^2}}(|\overline{L}\rangle + |\overline{U}\rangle + \alpha|\overline{M}\rangle), \tag{A50}$$

where $\overline{X}$ means a vacant site on the rung at position X. The matrix element $\langle\Psi_1|H^{\rm leg}_{\rm kin}|\Psi_2\rangle$ now involves the initial and final states,

$$\begin{aligned}
|\Psi_1\rangle &= |s\rangle\otimes|d\rangle \\
&= \frac{1}{2\sqrt{2+\alpha^2}}\Big(|U\overline{U}\rangle+\sqrt{2}|M\overline{U}\rangle+|L\overline{U}\rangle+\alpha|U\overline{M}\rangle+\sqrt{2}\alpha|M\overline{M}\rangle+\alpha|L\overline{M}\rangle+|U\overline{L}\rangle+\sqrt{2}|M\overline{L}\rangle+|L\overline{L}\rangle\Big) \quad \text{(A51)}\\
|\Psi_2\rangle &= |d\rangle\otimes|s\rangle \\
&= \frac{1}{2\sqrt{2+\alpha^2}}\Big(|\overline{U}U\rangle+\sqrt{2}|\overline{U}M\rangle+|\overline{U}L\rangle+\alpha|\overline{M}U\rangle+\sqrt{2}\alpha|\overline{M}M\rangle+\alpha|\overline{M}L\rangle+|\overline{L}U\rangle+\sqrt{2}|\overline{L}M\rangle+|\overline{L}L\rangle\Big) \quad \text{(A52)}
\end{aligned}$$

After expanding both sides one gets,

$$\begin{aligned}
\langle\Psi_1|H^{\rm leg}_{\rm kin}|\Psi_2\rangle &= \frac{1}{4(2+\alpha^2)}\Big(\langle\overline{L}L|H^{\rm leg}_{\rm kin}|U\overline{U}\rangle+\sqrt{2}\alpha\langle\overline{M}M|H^{\rm leg}_{\rm kin}|U\overline{U}\rangle+2\langle\overline{U}M|H^{\rm leg}_{\rm kin}|M\overline{U}\rangle \\
&+ \langle\overline{U}L|H^{\rm leg}_{\rm kin}|L\overline{U}\rangle+\alpha^2\langle\overline{M}U|H^{\rm leg}_{\rm kin}|U\overline{M}\rangle+\sqrt{2}\alpha\langle\overline{L}L|H^{\rm leg}_{\rm kin}|M\overline{M}\rangle \\
&+ \sqrt{2}\alpha\langle\overline{U}U|H^{\rm leg}_{\rm kin}|M\overline{M}\rangle+\alpha^2\langle\overline{M}L|H^{\rm leg}_{\rm kin}|L\overline{M}\rangle+\langle\overline{L}U|H^{\rm leg}_{\rm kin}|U\overline{L}\rangle \\
&+ 2\langle\overline{L}M|H^{\rm leg}_{\rm kin}|M\overline{L}\rangle+\sqrt{2}\alpha\langle\overline{M}M|H^{\rm leg}_{\rm kin}|L\overline{L}\rangle+\langle\overline{U}U|H^{\rm leg}_{\rm kin}|L\overline{L}\rangle\Big). \quad \text{(A53)}
\end{aligned}$$

The contributions of the individual terms are as follows:

$$\begin{aligned}
\langle\overline{L}L|H^{\rm leg}_{\rm kin}|U\overline{U}\rangle &= \langle\overline{U}U|H^{\rm leg}_{\rm kin}|L\overline{L}\rangle=\phi^{-1}t_{\rm leg}\langle\mathbf{1}\tau|h_{\rm kin}|\tau\mathbf{1}\rangle,\\
\langle\overline{M}M|H^{\rm leg}_{\rm kin}|U\overline{U}\rangle &= \langle\overline{U}M|H^{\rm leg}_{\rm kin}|M\overline{U}\rangle=\langle\overline{L}U|H^{\rm leg}_{\rm kin}|U\overline{L}\rangle=e^{4\pi i/5}\phi^{-1}t_{\rm leg}\langle\mathbf{1}\tau|h_{\rm kin}|\tau\mathbf{1}\rangle,\\
\langle\overline{L}L|H^{\rm leg}_{\rm kin}|M\overline{M}\rangle &= \langle\overline{U}L|H^{\rm leg}_{\rm kin}|L\overline{U}\rangle=\langle\overline{M}M|H^{\rm leg}_{\rm kin}|L\overline{L}\rangle=e^{-4\pi i/5}\phi^{-1}t_{\rm leg}\langle\mathbf{1}\tau|h_{\rm kin}|\tau\mathbf{1}\rangle,\\
\langle\overline{M}U|H^{\rm leg}_{\rm kin}|U\overline{M}\rangle &= \langle\overline{U}U|H^{\rm leg}_{\rm kin}|M\overline{M}\rangle=e^{4\pi i/5}\phi^{-1}t_{\rm leg}\langle\mathbf{1}\tau|h_{\rm kin}|\tau\mathbf{1}\rangle,\\
\langle\overline{M}L|H^{\rm leg}_{\rm kin}|L\overline{M}\rangle &= \langle\overline{L}M|H^{\rm leg}_{\rm kin}|M\overline{L}\rangle=e^{-4\pi i/5}\phi^{-1}t_{\rm leg}\langle\mathbf{1}\tau|h_{\rm kin}|\tau\mathbf{1}\rangle. \quad \text{(A54)}
\end{aligned}$$

Replacing (A54) into (A53) one gets the effective hopping,

$$\begin{aligned}
t &= \frac{\langle\Psi_1|H^{\rm leg}_{\rm kin}|\Psi_2\rangle}{\langle\mathbf{1}\tau|h_{\rm kin}|\tau\mathbf{1}\rangle} \\
&= \frac{1}{(2+\alpha^2)2\phi}\Big[(3+\alpha^2+2\sqrt{2}\alpha)\Big(\cos\frac{4\pi}{5}\Big)+1\Big]t_{\rm leg}
\end{aligned} \quad \text{(A55)}$$

Heavy hole – super-heavy τ : The third case corresponds to the effective hole state $|d\rangle$ defined in (A50) and the effective τ particle state defined by the fully occupied rung $|f\rangle=|3,\tau\rangle$. The initial and final states $|\Psi_1\rangle$ and $|\Psi_2\rangle$ are now given by :

$$\begin{aligned}
|\Psi_1\rangle &= |d\rangle\otimes|f\rangle \\
&= \frac{1}{\sqrt{2+\alpha^2}}\Big(|\overline{U}f\rangle+\alpha|\overline{M}f\rangle+|\overline{L}f\rangle\Big), \quad \text{(A56)}\\
|\Psi_2\rangle &= |f\rangle\otimes|d\rangle \\
&= \frac{1}{\sqrt{2+\alpha^2}}\Big(|f\overline{U}\rangle+\alpha|f\overline{M}\rangle+|f\overline{L}\rangle\Big). \quad \text{(A57)}
\end{aligned}$$

The matrix element for the kinetic Hamiltonian on the legs is now expressed as :

$$\begin{aligned}
\langle\Psi_2|H^{\rm leg}_{\rm kin}|\Psi_1\rangle &= \frac{1}{2+\alpha^2}\Big(\langle f\overline{U}|H^{\rm leg}_{\rm kin}|\overline{U}f\rangle \\
&+ \alpha^2\langle f\overline{M}|H^{\rm leg}_{\rm kin}|\overline{M}f\rangle \\
&+ \langle f\overline{L}|H^{\rm leg}_{\rm kin}|\overline{L}f\rangle\Big). \quad \text{(A58)}
\end{aligned}$$

The individual contributions of these terms are:

$$\begin{aligned}
\langle f\overline{U}|H^{\rm leg}_{\rm kin}|U\overline{f}\rangle &= \phi^{-2}t_{\rm leg}\langle\mathbf{1}\tau|h_{\rm kin}|\tau\mathbf{1}\rangle,\\
\langle f\overline{M}|H^{\rm leg}_{\rm kin}|M\overline{f}\rangle &= \Big(\frac{1}{2\phi}+\phi^{-3}\Big)t_{\rm leg}\langle\mathbf{1}\tau|h_{\rm kin}|\tau\mathbf{1}\rangle,\\
\langle f\overline{L}|H^{\rm leg}_{\rm kin}|L\overline{f}\rangle &= t_{\rm leg}\langle\mathbf{1}\tau|h_{\rm kin}|\tau\mathbf{1}\rangle. \quad \text{(A59)}
\end{aligned}$$

Adding the contributions of the three terms we get:

$$\begin{aligned}
t &= \frac{\langle\Psi_2|H^{\rm leg}_{\rm kin}|\Psi_1\rangle}{\langle\mathbf{1}\tau|h_{\rm kin}|\tau\mathbf{1}\rangle} \\
&= \frac{1}{2+\alpha^2}\Big[\frac{1}{\phi^2}+\frac{\alpha^2}{2\phi}+\frac{\alpha^2}{\phi^3}+1\Big]t_{\rm leg}.
\end{aligned} \quad \text{(A60)}$$

Super-heavy hole – heavy τ : The fourth case corresponds to a τ in the state $|2^{\pm},\tau\rangle$ defined in Eq. (A22). The effective hole on the ladder is defined by the fully occupied state $|f\rangle \equiv |3,\mathbf{1}\rangle$. We calculate the matrix element of the states

$$\begin{aligned} |\Psi_1\rangle &= |2^{\pm},\tau\rangle \otimes |f\rangle \\ &\equiv \frac{1}{2}\big(|UM,f\rangle + |ML,f\rangle \pm \sqrt{2}|UL,f\rangle\big) \quad \text{(A61)} \end{aligned}$$

and

$$\begin{aligned} |\Psi_2\rangle &= |f\rangle \otimes |2^{\pm},\tau\rangle \\ &\equiv \frac{1}{2}\big(|f,UM\rangle + |f,ML\rangle \pm \sqrt{2}|f,UL\rangle\big). \quad \text{(A62)} \end{aligned}$$

The matrix elements are given by

$$\begin{aligned} \langle\Psi_2|H^{\rm leg}_{\rm kin}|\Psi_1\rangle &= \frac{1}{4}\big(\langle f,UM|H^{\rm leg}_{\rm kin}|UM,f\rangle \\ &+ \langle f,ML|H^{\rm leg}_{\rm kin}|ML,f\rangle \\ &+ 2\langle f,UL|H^{\rm leg}_{\rm kin}|UL,f\rangle\big). \quad \text{(A63)} \end{aligned}$$

The contributions of the individual hopping terms are

$$\begin{aligned} \langle f,UM|H^{\rm leg}_{\rm kin}|UM,f\rangle &= \phi^{-1}e^{6\pi i/5}\langle \mathbf{1}\tau|h_{\rm kin}|\tau\mathbf{1}\rangle, \\ \langle f,UL|H^{\rm leg}_{\rm kin}|UL,f\rangle &= \phi^{-1}e^{-6\pi i/5}\langle \mathbf{1}\tau|h_{\rm kin}|\tau\mathbf{1}\rangle, \\ \langle f,ML|H^{\rm leg}_{\rm kin}|ML,f\rangle &= \phi^{-1}\langle \mathbf{1}\tau|h_{\rm kin}|\tau\mathbf{1}\rangle. \quad \text{(A64)} \end{aligned}$$

Using Eqs. A64 in Eq. (A63), we get

$$\begin{aligned} t &= \frac{\langle\Psi_2|H^{\rm leg}_{\rm kin}|\Psi_1\rangle}{\langle \mathbf{1}\tau|h_{\rm kin}|\tau\mathbf{1}\rangle} \\ &= \left(\frac{1}{2\phi}-\frac{1}{4}\right)t_{\rm leg}. \quad \text{(A65)} \end{aligned}$$

Light τ – Heavy τ : Finally, we consider two rungs with a light τ defined by the state $|s\rangle$ in (A18) and a heavy τ defined by the state $|h\rangle$ given as :

$$|h\rangle = \frac{1}{2}(|\overline{L}\rangle + \sqrt{2}|\overline{M}\rangle + |\overline{U}\rangle). \quad \text{(A66)}$$

The initial and final states, formed by the tensor product of $|s\rangle$ and $|h\rangle$ are defined as:

$$\begin{aligned} |\Psi_1\rangle &= |s\rangle \otimes |h\rangle \\ &= \frac{1}{4}\Big(|U\overline{U}\rangle + \sqrt{2}|M\overline{U}\rangle + |L\overline{U}\rangle \\ &+ \sqrt{2}|U\overline{M}\rangle + 2|M\overline{M}\rangle + \sqrt{2}|L\overline{M}\rangle \\ &+ |U\overline{L}\rangle + \sqrt{2}|M\overline{L}\rangle + |L\overline{L}\rangle\Big) \quad \text{(A67)} \end{aligned}$$

and,

$$\begin{aligned} |\Psi_2\rangle &= |h\rangle \otimes |s\rangle \\ &= \frac{1}{4}\Big(|\overline{U}U\rangle + \sqrt{2}|\overline{U}M\rangle + |\overline{U}L\rangle \\ &+ \sqrt{2}|\overline{M}U\rangle + \sqrt{2}|\overline{M}M\rangle + \sqrt{2}|\overline{M}L\rangle \\ &+ |\overline{L}U\rangle + \sqrt{2}|\overline{L}M\rangle + |\overline{L}L\rangle\Big). \quad \text{(A68)} \end{aligned}$$

The matrix elements corresponding to the hopping along the leg on the ladder can be expanded using the expression of the states to give :

$$\begin{aligned} \langle\Psi_1|H^{\rm leg}_{\rm kin}|\Psi_2\rangle &= \frac{1}{16}\Big(\langle\overline{L}L|H^{\rm leg}_{\rm kin}|U\overline{U}\rangle + 2\langle\overline{M}M|H^{\rm leg}_{\rm kin}|U\overline{U}\rangle + 2\langle\overline{U}M|H^{\rm leg}_{\rm kin}|M\overline{U}\rangle + \langle\overline{U}L|H^{\rm leg}_{\rm kin}|L\overline{U}\rangle \\ &+ 2\langle\overline{M}U|H^{\rm leg}_{\rm kin}|U\overline{M}\rangle + 2\langle\overline{L}L|H^{\rm leg}_{\rm kin}|M\overline{M}\rangle + 2\langle\overline{U}U|H^{\rm leg}_{\rm kin}|M\overline{M}\rangle + 2\langle\overline{M}L|H^{\rm leg}_{\rm kin}|L\overline{M}\rangle \\ &+ \langle\overline{L}U|H^{\rm leg}_{\rm kin}|U\overline{L}\rangle + 2\langle\overline{L}M|H^{\rm leg}_{\rm kin}|M\overline{L}\rangle + 2\langle\overline{M}M|H^{\rm leg}_{\rm kin}|L\overline{L}\rangle + \langle\overline{U}U|H^{\rm leg}_{\rm kin}|L\overline{L}\rangle\Big). \quad \text{(A69)} \end{aligned}$$

The contributions of the individual terms are as follows:

$$\begin{aligned} \langle\overline{L}L|H^{\rm leg}_{\rm kin}|U\overline{U}\rangle &= \langle\overline{U}U|H^{\rm leg}_{\rm kin}|L\overline{L}\rangle = t_{\rm leg}\langle \mathbf{1}\tau|h_{\rm kin}|\tau\mathbf{1}\rangle, \\ \langle\overline{M}M|H^{\rm leg}_{\rm kin}|U\overline{U}\rangle &= \langle\overline{U}M|H^{\rm leg}_{\rm kin}|M\overline{U}\rangle = \langle\overline{L}U|H^{\rm leg}_{\rm kin}|U\overline{L}\rangle = t_{\rm leg}e^{-3\pi i/5}\langle \mathbf{1}\tau|h_{\rm kin}|\tau\mathbf{1}\rangle, \\ \langle\overline{U}L|H^{\rm leg}_{\rm kin}|L\overline{U}\rangle &= \langle\overline{L}L|H^{\rm leg}_{\rm kin}|M\overline{M}\rangle = \langle\overline{M}L|H^{\rm leg}_{\rm kin}|L\overline{M}\rangle = t_{\rm leg}e^{3\pi i/5}\langle \mathbf{1}\tau|h_{\rm kin}|\tau\mathbf{1}\rangle, \\ \langle\overline{M}U|H^{\rm leg}_{\rm kin}|U\overline{M}\rangle &= \langle\overline{U}U|H^{\rm leg}_{\rm kin}|M\overline{M}\rangle = t_{\rm leg}e^{-3\pi i/5}\langle \mathbf{1}\tau|h_{\rm kin}|\tau\mathbf{1}\rangle, \\ \langle\overline{M}M|H^{\rm leg}_{\rm kin}|L\overline{L}\rangle &= \langle\overline{L}M|H^{\rm leg}_{\rm kin}|M\overline{L}\rangle = t_{\rm leg}e^{3\pi i/5}\langle \mathbf{1}\tau|h_{\rm kin}|\tau\mathbf{1}\rangle. \quad \text{(A70)} \end{aligned}$$

Replacing (A70) into (A69) one gets the effective hopping,

$$t = \frac{\langle\Psi_1|H^{\rm leg}_{\rm kin}|\Psi_2\rangle}{\langle \mathbf{1}\tau|h_{\rm kin}|\tau\mathbf{1}\rangle} = \frac{1}{8}\big[1+9\cos(3\pi/5)\big]t_{\rm leg}. \quad \text{(A71)}$$

3. Higher order terms

In addition to the above cases, we can also have a kinetic and potential terms when the difference in the $U(1)$ charges on neighboring rungs is larger than 1. Such process occurs e.g. (i) between a charge-0 (light) hole and a charge-2 (heavy) hole (marked by blue arrows in Table. V) in the P_2 paired phase or (ii) between a charge-0 (light) hole and a charge-3 (super heavy) τ (marked by orange arrows in Table. V) in the PS_{03} phase.

In case (i), one needs to hop twice to be able to come back to a configuration $|\Psi_J\rangle$ that has the same $U(1)$ charges as the initial configuration $|\Psi_I\rangle$, so the effective Hamiltonian (leaving in the relevant subspace) is obtained in second-order perturbation, in $t_{\rm leg}$[61,62]

$$\langle\Psi_I|H_{\rm eff}|\Psi_J\rangle = -\sum_r \frac{\langle\Psi_I|H^{\rm leg}_{\rm kin}|\Psi_r\rangle\langle\Psi_r|H^{\rm leg}_{\rm kin}|\Psi_J\rangle}{E_r - E_J}, \quad \text{(A72)}$$

where the sum is on the intermediate states corresponding to two (light) τ's on neighboring sites. The energy denominator is given by $E_D = (-2t_{\rm rung} + J_{\rm rung})$ and matrix elements for all the intermediate states are $(-t_{\rm leg})$ so that one gets for $I = J$ a potential energy

$$V = -\frac{2t^2_{\rm leg}}{E_D} \quad \text{(A73)}$$

and for $I \neq J$ a hopping term

$$t = -\frac{2t^2_{\rm leg}}{E_D}. \quad \text{(A74)}$$

In case (ii), one needs to hop three times to be able to come back to a configuration that has the same $U(1)$ charges as the initial configuration, so the effective Hamiltonian is now obtained in third-order perturbation in $t_{\rm leg}$:[61,62]

$$\langle\Psi_I|H_{\rm eff}|\Psi_J\rangle = \sum_{r,s} \frac{\langle\Psi_I|H^{\rm leg}_{\rm kin}|\Psi_r\rangle\langle\Psi_r|H^{\rm leg}_{\rm kin}|\Psi_s\rangle\langle\Psi_s|H^{\rm leg}_{\rm kin}|\Psi_J\rangle}{(E_s - E_J)(E_r - E_J)}, \quad \text{(A75)}$$

where the intermediate states $|\Psi_r\rangle$ and $|\Psi_s\rangle$ carry a heavy hole and a light τ on neighboring rungs. The energy denominators given by the difference in energy between the initial (degenerate with the final) state and the intermediate states thus take the value

$$E_D = (\phi - \frac{1}{2})J_{\rm rung} - \sqrt{2}t_{\rm rung} - \frac{\sqrt{J^2_{\rm rung} + 8t^2_{\rm rung}}}{2}. \quad \text{(A76)}$$

Starting from an initial state $|3,\tau\rangle\otimes|e\rangle$ a simple hopping yields the intermediate state $|2,\mathbf{1}\rangle\otimes|1,\tau\rangle$ with the matrix elements given by for hopping on the upper leg

$$t^1_U = \phi^{-1}t_{\rm leg}, \quad \text{(A77)}$$

on the middle leg,

$$t^1_M = \phi^{-1}e^{-4i\pi/5}t_{\rm leg}, \quad \text{(A78)}$$

and on the lower leg,

$$t^1_L = t_{\rm leg}\,. \quad \text{(A79)}$$

Subsequently, a second hopping yields the intermediate state $|1,\tau\rangle\otimes|2,\mathbf{1}\rangle$ with hopping matrix elements on the upper leg

$$t^2_U = \phi^{-1}e^{-4i\pi/5}t_{\rm leg}, \quad \text{(A80)}$$

on the middle leg,

$$t^2_M = \phi^{-1}t_{\rm leg}, \quad \text{(A81)}$$

and on the lower leg,

$$t^2_L = \phi^{-1}e^{4i\pi/5}t_{\rm leg}\,. \quad \text{(A82)}$$

Finally to come back to a state carrying the same $U(1)$ charges on the rungs, the hopping amplitudes for the three legs are just the complex conjugate of those described in Eqs. (A77)-(A79), thus giving for $I = J$ a potential energy

$$V = \frac{(2\phi^{-2}+1)t^2_{\rm leg}}{E_D} \quad \text{(A83)}$$

and for $I \neq J$ a hopping term

$$t = \frac{t^3_{\rm leg}}{E^2_D}(3\phi^{-2} + 2\phi^{-3} + \phi^{-2}e^{8\pi i/5}). \quad \text{(A84)}$$

Appendix B: Implementation details

In this section we describe briefly as to how we generate the Hilbert space for anyonic systems and the Hamiltonian numerically.

1. Hilbert space

The model of doped Fibonacci ladders is described in terms of two quantum numbers : the $U(1)$ charge and the anyonic spin. The most homogenous way to represent this system would be to keep information about both these quantum numbers on the bond labels of the fusion tree. However, since the $U(1)$ charge is Abelian and counts the number of anyons in the system, it is advantageous to label it separately. Thus, the system is described by a fusion tree with two labels, one for each of the quantum numbers. The $U(1)$ charge is labeled by the position of the anyons on the sites and the non-Abelian anyonic spin is labeled by the bond labels of the fusion tree.

We first need to store the basis states of the Hilbert space. We can compactly store the configuration by means of two separate integers, one each for the $U(1)$ charge (site labels) and non-Abelian charge (bond labels). Each bit of these integers represents a single site (or bond) label which is set to 1 if an anyon is present on that particular site (or bond), otherwise is set to 0. The bond labels of the fusion tree are constrained by the fusion rules that must be satisfied on each trivalent vertex.

Since the model conserves the number of particles in the system, the total number of 0's and 1's in the integers for the $U(1)$ charge must be fixed in the system for a given particle density. Say, for example, we have a system of L sites with N particles. The integers for the site labels, hence, carry L bits. The set of site labels contains all those integers that have exactly N out of L bits set to 1. Let us call $\mathcal{S}$ the set that contains all the possible states for the site labels consistent with the number of anyons in the system. Further for each element in $\mathcal{S}$, we enumerate all allowed configurations for the bond labels by imposing the fusion rules at every trivalent vertex of the fusion tree. The states for the bond labels belong to the set $\mathcal{B}\big(|\psi_{\text{site}}\rangle\big)$ that is defined by the site labels.

We illustrate this method of writing the states in the Hilbert space for a section of the fusion path with two vacant sites and two anyons ($L = 4, N = 2$). In figure B 1, we show two possible configurations for this case. The site labels are represented by blue (anyons) and white (holes) circles. The bond labels, x_i, are shown by red circles. The holes may be present on any two of the four sites, however we must record the information about their position since different site labels correspond to a different set of bond labels.

For example in figure B 1(a) the state for the site charges would read $|\psi^a_{\text{site}}\rangle = |0011\rangle$ but for figure B 1(b) the corresponding state would be $|\psi^b_{\text{site}}\rangle = |0101\rangle$. Owing to the non-Abelian nature of the theory, for each of these site configurations we obtain several configurations for the bond labels that are consistent with the fusion rules.

For example, for the case B 1(a) the bond labels

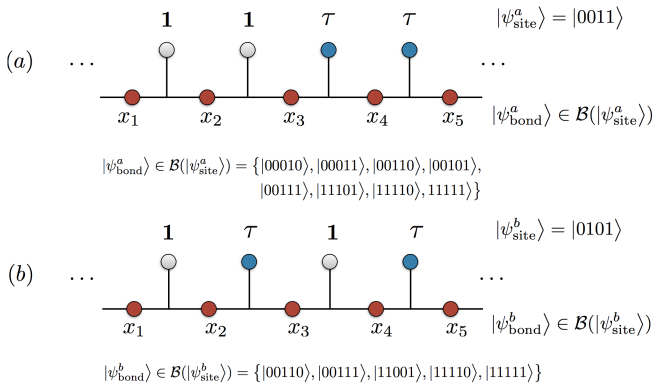

FIG. 24: Illustration of the Hilbert space for two possible site configurations for a section of the fusion path with two particles and two vacant sites. The state for the site labels is (a) $|\psi^a_{\text{site}}\rangle = |0011\rangle$ and (b) $|\psi^b_{\text{site}}\rangle = |0101\rangle$. The state for the bond labels is $|\psi_{\text{bond}}\rangle = |x_1x_2x_3x_4x_5\rangle \in \mathcal{B}(|\psi_{\text{site}}\rangle)$.

$|\psi^a_{\text{bond}}\rangle$ belong to the set

$$|\psi^a_{\text{bond}}\rangle \in \mathcal{B}(|\psi^a_{\text{site}}\rangle) = \big\{|00010\rangle, |00011\rangle, |00110\rangle, |00101\rangle, |00111\rangle, |11101\rangle, |11110\rangle, 11111\rangle\big\} \tag{B1}$$

whereas for the case B 1(b) the bond labels $|\psi^b_{\text{bond}}\rangle$ belong to the set

$$|\psi^b_{\text{bond}}\rangle \in \mathcal{B}(|\psi^b_{\text{site}}\rangle) = \big\{|00110\rangle, |00111\rangle, |11001\rangle, |11110\rangle, |11111\rangle\big\}. \tag{B2}$$

The full quantum state is described by taking into account both $|\psi_{\text{site}}\rangle$ and $|\psi_{\text{bond}}\rangle$. Thus, the Hilbert space $\mathcal{H}$ is defined by the set $\{|\psi_{\text{site}}\rangle \otimes |\psi_{\text{bond}}\rangle\}$: $|\psi_{\text{site}}\rangle \in \mathcal{S}, |\psi_{\text{bond}}\rangle \in \mathcal{B}(|\psi_{\text{site}}\rangle)$. Note that for a golden chain/ladder ($\rho = 1$) the state describing the site labels becomes redundant since all the site labels are identically equal to 1.

Further, our system has a translation symmetry, i.e. it remains invariant if the site and bond labels are shifted by a certain amount. This enables us to write the wavefunctions as Bloch waves labeled by the momentum. The Hamiltonian becomes a block-diagonal operator and each of these blocks can be diagonalized individually. The Hilbert space is reduced by a factor of L, making the numerics much more tractable.

In Table VI, we list the sizes of the Hilbert space (in the $K = 0$ sector) for doped ladders. The Hilbert space sizes for their corresponding effective models are listed in Table VII. Additionally in Table VIII, we mention the Hilbert space sizes of the largest chains we simulated for the heavy-light model.

TABLE VI: Hilbert space sizes for doped ladders of Fibonacci anyons without charging energy.

W	L	Filling	Size of Hilbert space
2	8	$\rho = 3/4$	73322
3	6	$\rho = 5/18$	15708

TABLE VII: Hilbert space sizes for effective models of doped Fibonacci ladders.

L	Filling	Model	Size of Hilbert space
8	$\tilde{\rho} = 1/2$	$t-J$	64
6	$\tilde{\rho} = 5/6$	$t-J$	11

TABLE VIII: Hilbert space sizes for effective 1D chains of the heavy-light model.

L	Filling	Model	Size of Hilbert space
8	$\tilde{\rho} = 1/2$	heavy-light	418
20	$\tilde{\rho} = 1/2$	heavy-light	139741760
20	$\tilde{\rho} = 1/4$	heavy-light	11726456

2. Generating the Hamiltonian

Local interactions are treated simply by multiplying the wavefunction with the Hamiltonian for the interaction. For our choice of fusion path, leg interactions defined in Eqs. (14) - (18) (see main text) are longer range interactions, thus involving Braid matrices in addition to the interaction term. Note that since the Braid matrix can generate up to two states per bond, we can obtain up to 2^{2W-1} states for magnetic interactions and 2^{2W-2} states for kinetic terms. The non-zero entries for each row of the Hamiltonian matrix are thus growing exponentially with the width of the ladder giving rise to a dense matrix for the Hamiltonian. The action of this dense Hamiltonian on the wavefunction would turn out to be numerically expensive. So, instead of multiplying a single matrix with an exponentially large number of non-zero elements with the wavefunction, we implement the same process by iteratively multiplying the wavefunction by $2W-1$ sparse matrices as follows. We multiply the wavefunction successively with the Braid matrices, the number of braids depending on W. Thereafter, we treat the local interaction term. Subsequently we act one by one with all the inverse braid matrices to obtain the final wavefunction. The Hamiltonian is thus generated by successive multiplication of $W-1$ Braid matrices followed by multiplication with the interaction term and finally by $W-1$ inverse Braid matrices. Since the matrix is becoming denser with the width of the ladder, the exact diagonalization becomes more and more computationally expensive and we can treat only medium sized systems numerically.

[1] J. M. Leinaas and J. Myrheim, On the theory of identical particles, Nuovo Cimento **37B**, 1 (1977).

[2] F. Wilczek, Quantum Mechanics of Fractional-Spin Particles, Phys. Rev. Lett. **49**, 957 (1982).

[3] G. S. Canright and S. M. Girvin, Fractional statistics: quantum possibilities in two dimensions, Science **247**, 1197 (1990).

[4] K. Fredenhagen, K. H. Rehren, and B. Schroer, Superselection sectors with braid group statistics and exchange algebras, Commun. Math. Phys. **125**, 201 (1989).

[5] J. Fröhlich and F. Gabbiani, Braid statistics in local quantum theory, Rev. Math. Phys. **2**, 251 (1990).

[6] D. J. Clarke, J. Alicea, and K. Shtengel, Exotic non-Abelian anyons from conventional fractional quantum Hall states, Nature Commun. **4**, 1348 (2013).

[7] G. Moore and N. Read, Nonabelions in the fractional quantum hall effect, Nucl. Phys. B **360**, 362 (1991).

[8] N. Read and E. Rezayi, Beyond paired quantum Hall states: Parafermions and incompressible states in the first excited Landau level, Phys.Rev. B **59**, 8084 (1999).

[9] D. J. Clarke, J. Alicea, and K. Shtengel, Exotic circuit elements from zero-modes in hybrid superconductor-quantum-Hall systems, Nat Phys **10**, 877 (2014).

[10] J. Alicea, Y, Oreg, G. Refael, F. V. Oppen, and M. P. A. Fisher, Non-Abelian statistics and topological quantum information processing in 1D wire networks, Nat Phys **7**, 412 (2011).

[11] M. A. Levin and X.-G. Wen, String-net condensation: A physical mechanism for topological phases, Phys. Rev. B **71**, 045110 (2005).

[12] N. E. Bonesteel and D. P. DiVincenzo, Quantum circuits for measuring Levin-Wen operators, Phys. Rev. B **86**, 165113 (2012).

[13] E. Kapit and S. Simon, Three- and four-body interactions from two-body interactions in spin models: A route to Abelian and non-Abelian fractional Chern insulators, Phys. Rev. B **88**, 184409 (2013).

[14] G. Palumbo and J. K. Pachos, Non-Abelian Chern-Simons theory from a Hubbard-like model , Phys. Rev. D **90**, 027703 (2014).

[15] N. Read and D. Green, Paired states of fermions in two dimensions with breaking of parity and time-reversal symmetries and the fractional quantum Hall effect, Phys. Rev. B **61**, 10267 (2000).

[16] A.Yu. Kitaev, Unpaired Majorana fermions in quantum wires, Phys.-Usp. **44**, 131 (2001) ; cond-mat/0010440.

[17] L. Fu and C. L. Kane, Superconducting Proximity Effect and Majorana Fermions at the Surface of a Topological Insulator, Phys. Rev. Lett. **100**, 096407 (2008).

[18] J. D. Sau, R. M. Lutchyn, S. Tewari, S. Das Sarma, Generic

New Platform for Topological Quantum Computation Using Semiconductor Heterostructures, Phys. Rev. Lett. **104**, 040502 (2010).

[19] R. M. Lutchyn, J. D. Sau, S. Das Sarma, Majorana Fermions and a Topological Phase Transition in Semiconductor-Superconductor Heterostructures, Phys. Rev. Lett. 105, 077001 (2010).

[20] R. S. K. Mong, D. J. Clarke, J. Alicea, N. H. Lindner, P. Fendley, C. Nayak, Y. Oreg, A. Stern, E. Berg, K. Shtengel, and M. P. A. Fisher, Universal topological quantum computation from a superconductor/Abelian quantum Hall heterostructure, Phys. Rev. X **4**, 011036 (2014).

[21] N.R. Cooper, N.K. Wilkin, and J.M.F. Gunn, Quantum Phases of Vortices in Rotating Bose-Einstein Condensates, Phys. Rev. Lett. **87**, 120405 (2001).

[22] J. K. Slingerland and F. A. Bais, Quantum groups and nonabelian braiding in quantum Hall systems, Nucl. Phys. B **612**, 229 (2001).

[23] V. Mourik, K. Zuo, S. M. Frolov, S. R. Plissard, E. P. A. M. Bakkers, and L. P. Kouwenhoven, Signatures of Majorana Fermions in Hybrid Superconductor-Semiconductor Nanowire Devices, Science **336**, 1003 (2012).

[24] A. Das, Y. Ronen, Y. Most, Y. Oreg, M. Heiblum, and H. Shtrikman, Zero-bias peaks and splitting in an Al-InAs nanowire topological superconductor as a signature of Majorana fermions, Nat. Phys. **8**, 887 (2012).

[25] L. P. Rokhinson, X. Liu, and J. K. Furdyna, The fractional ac Josephson effect in a semiconductor-superconductor nanowire as a signature of Majorana particles, Nat. Phys. **8**, 795 (2012).

[26] A. D. K. Finck, D. J. Van Harlingen, P. K. Mohseni, K. Jung, and X. Li, Anomalous Modulation of a Zero-Bias Peak in a Hybrid Nanowire-Superconductor Device, Phys. Rev. Lett. **110**, 126406 (2013).

[27] H. O. H. Churchill, V. Fatemi, K. Grove-Rasmussen, M. T. Deng, P. Caroff, H. Q. Xu, and C. M. Marcus, Superconductor-nanowire devices from tunneling to the multichannel regime: Zero-bias oscillations and magnetoconductance crossover, Phys. Rev. B **87**, 241401 (2013).

[28] J. Preskill, Introduction to Quantum Computation, (World Scientific, 1998), quant-ph/9712048.

[29] A. Stern and N. H. Lindner, Topological Quantum Computation-From Basic Concepts to First Experiments, Science, **339**, 1179 (2013).

[30] C. Nayak, S.H. Simon, A. Stern, M. Freedman, and S. Das Sarma, Non-Abelian anyons and topological quantum computation, Rev. Mod. Phys. **80**, 1083 (2008).

[31] M. Freedman, A. Kitaev, M. Larsen and Z. Wang, Topological quantum computation, Bull. Amer. Math. Soc. **40**, 31-38 (2003).

[32] A. Y. Kitaev, Fault-tolerant quantum computation by anyons, Ann. Phys. **303**, 2 (2003).

[33] A. Kitaev, Anyons in an exactly solved model and beyond, Ann. Phys. **321**, 2, (2006).

[34] S. Trebst, M. Troyer, Z. Wang, and A. W. W. Ludwig, A Short Introduction to Fibonacci Anyon Models, Prog. Theo. Phys. Supp. **176**, 384 (2008).

[35] A. Feiguin, S. Trebst, A. W. W. Ludwig, M. Troyer, A. Kitaev, Z. Wang, and M. Freedman, Interacting anyons in topological quantum liquids: The golden chain, Phys. Rev. Lett. **98**, 160409 (2007).

[36] S. Trebst, E. Ardonne, A. Feiguin, D. A. Huse, A. W. W. Ludwig, and M. Troyer, Collective States of Interacting Fibonacci Anyons, Phys. Rev. Lett. **101**, 050401 (2008).

[37] C. Gils, E. Ardonne, S. Trebst, A. W. W.Ludwig, M. Troyer, and Z. Wang, Collective states of interacting anyons, edge states, and the nucleation of topological liquids, Phys. Rev. Lett. **103**, 070401 (2009).

[38] C. Gils, E. Ardonne, S. Trebst, A. W. W.Ludwig, M. Troyer, and Z. Wang, Anyonic quantum spin chains: Spin-1 generalizations and topological stability, Phys. Rev. B **87**, 235120 (2013).

[39] P. E. Finch and H. Frahm, The $D(D3)$-anyon chain: integrable boundary conditions and excitation spectra, New J. Phys. **15**, 053035 (2013).

[40] P. E. Finch, M. Flohr, and H. Frahm, Integrable anyon chains: from fusion rules to face models to effective field theories, Nucl. Phys. B **889**, 299 (2014).

[41] P. E. Finch, H. Frahm, M. Lewerenz, A. Milsted, and T. J. Osborne, Quantum phases of a chain of strongly interacting anyons, Phys. Rev. B **90**, 081111(R) (2014).

[42] R. N. C. Pfeifer, O. Buerschaper, S. Trebst, A. W. W. Ludwig, M. Troyer, and G. Vidal, Translation invariance, topology, and protection of criticality in chains of interacting anyons, Phys. Rev. B **86**, 155111 (2012).

[43] N. E. Bonesteel and Kun Yang, Infinite-Randomness Fixed Points for Chains of Non-Abelian Quasiparticles, Phys. Rev. Lett. **99**, 140405 (2007).

[44] L. Fidkowski, G. Refael, N. E. Bonesteel, and J. E. Moore, c-theorem violation for effective central charge of infinite-randomness fixed points, Phys. Rev. B **78**, 224204 (2008).

[45] F.C. Zhang and T. M. Rice, Effective Hamiltonian for the superconducting Cu oxides, Phys. Rev. B **37**, 3759 (1988).

[46] J. Hubbard, Electron correlations in narrow energy bands, Proc. Roy. Soc. London A **276**, 238 (1963).

[47] M. C. Gutzwiller, Effect of Correlation on the Ferromagnetism of Transition Metals, Phys. Rev. Lett **10**, 159 (1963).

[48] J. Kanamori, Electron Correlation and Ferromagnetism of Transition Metals, Prog. of Theor. Phys. (Kyoto) **30**, 275 (1963).

[49] P. W. Anderson, Ground State of a Magnetic Impurity in a Metal, Phys. Rev. **164**, 352 (1967).

[50] D. Poilblanc, M. Troyer, E. Ardonne, and P. Bonderson, Fractionalization of Itinerant Anyons in One-Dimensional Chains, Phys. Rev. Lett. **108**, 207201 (2012).

[51] D. Poilblanc, A. Feiguin, M. Troyer, E. Ardonne, and P. Bonderson, One-dimensional itinerant interacting non-Abelian anyons, Phys. Rev. B **87**, 085106 (2013).

[52] S. Tomonaga, Remarks on Bloch's Method of Sound Waves applied to Many-Fermion Problems, Prog. Theor. Phys. **5**, 544 (1950).

[53] J. M. Luttinger, An Exactly Soluble Model of a Many-Fermion System, J. Math. Phys. Vol. **4**, 1154 (1963).

[54] F. D. M. Haldane, 'Luttinger liquid theory' of one-dimensional quantum fluids. I. Properties of the Luttinger model and their extension to the general 1D interacting spinless Fermi gas, J. Phys. C **14**, 2585 (1981).

[55] D. Poilblanc, A. W. W. Ludwig, S. Trebst, and M. Troyer, Quantum spin ladders of non-Abelian anyons, Phys. Rev. B **83**, 134439 (2011).

[56] A. W. W. Ludwig, D. Poilblanc, S. Trebst, and M. Troyer, Two-dimensional quantum liquids from interacting non-Abelian anyons, New J. Phys. **13**, 045014 (2011).

[57] E. Witten. Quantum field theory and the Jones polynomial. Commun. Math. Phys., **121** 351 1989.

[58] For basics on conformal field theory see, for example, P. Di Francesco, P. Mathieu, and D. Sénéchal, *Conformal Field*

Theory, Springer, New York (1997).

[59] For a review, see E. Dagotto and T. M. Rice, Surprises on the Way from One- to Two-Dimensional Quantum Magnets: The Ladder Materials, Science **271**, 618 (1996).

[60] M. Greven, R. J. Birgeneau, and U. -J. Wiese, Monte Carlo Study of Correlations in Quantum Spin Ladders, Phys. Rev. Lett. **77**, 1865 (1996).

[61] I. de P. R. Moreira, N. Suaud, N. Guihéry, J. P. Malrieu, R. Caballol, J. M. Bofill, and F. Illas, Derivation of spin Hamiltonians from the exact Hamiltonian: Application to systems with two unpaired electrons per magnetic site, Phys. Rev. B **66**, 134430 (2002).

[62] Jean Paul Malrieu, Rosa Caballol, Carmen J. Calzado, Coende Graaf, and Nathalie Guihéry, Magnetic Interactions in Molecules and Highly Correlated Materials: Physical Content, Analytical Derivation, and Rigorous Extraction of Magnetic Hamiltonians, Chem. Rev. **114**, 429-492 (2014).